Local Stochastic Volatility—The Hyp-Hyp Model

Nicholas Cowen

Supervisors:
Thomas McWalter
Jörg Kienitz

A dissertation submitted to the Faculty of Commerce, University of Cape Town, in partial fulfilment of the requirements for the degree of Master of Philosophy.

October 12, 2020

MPhil in Mathematical Finance,
University of Cape Town.

Declaration

I declare that this dissertation is my own, unaided work. It is being submitted for the Degree of Master of Philosophy in the University of the Cape Town. It has not been submitted before for any degree or examination in any other University.

October 12, 2020

Abstract

Volatility modelling is used predominantly in order to explain the volatility smile observed in the market. Stochastic volatility models are mainly used to capture the curvature of a volatility smile while local volatility models generally model the skew. Jäckel and Kahl (2008) present a hyperbolic-local hyperbolic-stochastic volatility (Hyp-Hyp) model which aims to improve upon existing local and stochastic volatility models such as the stochastic alpha, beta, rho (SABR) and constant elasticity of variance (CEV) models. The advantageous features of the Hyp-Hyp model are corroborated by implementing the model. Jäckel and Kahl (2008) investigate the accuracy of a scaled analytical approximation for implied volatility, based on approximations presented by Watanabe (1987) and Fouque *et al.* (2000), for the Hyp-Hyp model. They use the approximation to derive an expression for the delta of an option. This dissertation analyses the Hyp-Hyp model, as well as the approximation, by deriving expressions for other sensitivities and by investigating the effect of the Hyp-Hyp model parameters on the volatility smile. The accuracy of the analytical approximation for functional forms other than those defined by the Hyp-Hyp model is explored. A derivation of the approximation is undertaken, presenting corrections to the expressions introduced by Kahl (2007) and used by Jäckel and Kahl (2008).

Acknowledgements

I would like to thank my supervisors, Thomas McWalter and Jörg Kienitz, for their invaluable guidance, expertise and enthusiastic engagement.

I would also like to thank David Taylor and the rest of the AIFMRM staff for all that I have learnt and experienced this year.

Finally, I would like to thank my family for their support throughout my academic career and for always encouraging a love for learning.

Contents

List of Figures

Chapter 1

Introduction

Volatility modelling has become popular amongst academics and practitioners in recent years for a variety of reasons. It is often used to explain an observed model-implied volatility smile but is also used to model the impact of volatility changes on exotic derivatives that are particularly sensitive to these changes. Both local and stochastic volatility models attempt to describe the dynamics of volatility, thus providing a generalisation of the constant volatility assumption of the Black-Scholes model.

1.1 Stochastic Volatility

The introduction of stochastic volatility into a model allows one to describe an observed volatility smile by introducing uncertainty into the dynamics of volatility. It does this by modelling volatility as a stochastic process. Two popular stochastic volatility models are the Heston (1993) model and the stochastic alpha, beta, rho (SABR) model proposed by Hagan *et al.* (2002). Although the Heston model is widely used in practice, it may not always accurately match market dynamics, thus providing scope for new volatility models (Jäckel and Kahl, 2008). Indeed, the Heston model is so widely used predominantly because it is easily calibrated.

The SABR model better describes market-observed volatilities because it accurately captures the scaling of the "volatility of volatility" as a function of the level of volatility. The SABR model does, however, have shortcomings. It does not allow for mean reversion of volatility, nor does it permit for time-dependent parameters of the model. The lack of mean reversion is economically undesirable in that uncertainty in relative volatility grows over time. Another shortfall of the SABR dynamics is that higher order moments are not well defined. This can result in numerical implementation problems with regards to convergence.

1.2 Local Volatility

Local volatility attempts to describe the dynamics of volatility by defining it to be a deterministic function of time, t, and the value of the underlying, x_t. This is advantageous because it is often difficult to calibrate pure stochastic volatility models to short-term volatility smiles and skews. In practice, local volatility models are often used to capture the skew of a volatility smile, while stochastic volatility models are used to describe the curvature of the smile (Jäckel and Kahl, 2008).

Local volatility models are either parametric or non-parametric models. A non-parametric description of local volatility is one in which local volatility is given as a numerical solution to the Dupire (1994) equation. For example, if the price of a call option can be described as a function of maturity, T, and strike, K, the Dupire equation,

$$\sigma(T,K) = \frac{\sqrt{2}}{K}\sqrt{\frac{\frac{\partial C(T,K)}{\partial T} + rK\frac{\partial C(T,K)}{\partial K}}{\frac{\partial^2 C(T,K)}{\partial K^2}}}, \tag{1.1}$$

gives the local volatility, $\sigma(T,K)$.

The Dupire equation makes use of either interpolation or fitting of a parametric function to market-observable call prices to determine the partial derivatives needed in the equation. The same equation applies to put prices.

Parametric models are functional forms describing volatility as a function of t and x_t using parameters. For example, the constant elasticity of variance (CEV) model is defined as

$$dx_t = \sigma x_t^{\beta} dW_t,$$

where W_t is a standard Brownian motion and dx_t describes the forward dynamics of the underlying, x_t. The local volatility in the above equation is the coefficient of $x_t dW_t$ and is thus defined as $\sigma(t,x_t) = \sigma x_t^{\beta-1}$. This is a functional form of local volatility defined by the parameters β and σ. The displaced diffusion (DD) model is another example of a parametric local volatility model (Rubinstein, 1983).

Two popular parametric local volatility extensions to existing stochastic volatility models are those associated with the models mentioned above: the CEV and DD models. Under certain conditions, the CEV and DD models have the trait of allowing for the underlying to attain a value of zero, which, while acceptable for common interest rate derivatives, is undesirable in the pricing of derivatives on other assets such as stock indices. For $\beta < 1$, the CEV model can attain zero. The DD model can drop below zero if the displacement parameter is not specified to avoid this. The valuation of derivatives using a model that allows the underlying to attain zero is also economically undesirable. These undesirable traits are

described mathematically and discussed in Chapter 2.

This dissertation investigates the hyperbolic-local hyperbolic-stochastic volatility model, henceforth referred to as the Hyp-Hyp model. In Chapter 2, a review of literature, which describes the model, is conducted. Also presented are features of the Hyp-Hyp model that are deemed by Jäckel and Kahl (2008) to be advantageous when compared with the aforementioned existing volatility models. An analytical approximation, which was initially proposed by Kahl (2007), is also introduced in this chapter. Chapter 3 follows a similar structure to Chapter 2 because it explores in more detail the features of the model from Chapter 2 via the implementation of the model. Chapter 3 thus serves to detail the model implementation, fill in any gaps in the work done by Jäckel and Kahl (2008) and verify the results through the model implementation. Chapter 4 provides some new analysis by deriving expressions for sensitivities using the analytical approximation, analysing the Hyp-Hyp model parameters and exploring the accuracy of the approximation for functional forms that differ from those describing the Hyp-Hyp model. Finally, this dissertation provides a detailed derivation of the analytical approximations, which is presented in Appendix A.

Chapter 2

Literature Review

Jäckel and Kahl (2008) introduce the Hyp-Hyp model, which attempts to address the shortcomings of existing local stochastic volatility models discussed in Chapter 1. In addition to this, an analytical approximation for Black-Scholes implied volatilities of vanilla options is presented for two purposes: to increase the ease of calibration of the Hyp-Hyp model to market-observed volatility surfaces and to facilitate understanding of analytical features and sensitivities of the model.

2.1 The Hyp-Hyp Model

The Hyp-Hyp model is defined by the coupled system of stochastic differential equations (SDEs),

$$dx_t = \sigma_0 f(x_t) g(y_t) dW_t \tag{2.1}$$

and

$$dy_t = -\kappa y_t dt + \alpha\sqrt{2\kappa} dZ_t, \tag{2.2}$$

where x_t is the normalised value of the underlying asset (that is, $x_t = S_t/S_0$), y_t is the volatility driver and σ_0, α and κ are constant model parameters. The Brownian motions have a correlation, ρ, given by $\langle dW_t, dZ_t \rangle = \rho dt$. The initial condition for the volatility driver is $y_0 = 0$ and for the underlying is $x_0 = 1$. Hyperbolic functions,

$$f(x) = \frac{\left[\left(1-\beta+\beta^2\right)x + \left(\beta-1\right)\left(\sqrt{x^2+\beta^2\left(1-x\right)^2} - \beta\right)\right]}{\beta} \tag{2.3}$$

and

$$g(y) = y + \sqrt{y^2+1}, \tag{2.4}$$

describe the local and stochastic volatility structures of the model, respectively. The constant β is the local volatility parameter. It can be shown that the initial conditions correspond to function values of $g(0) = 1$ and $f(1) = 1$.

As defined above, the Hyp-Hyp model is a model of forward prices. The features of the hyperbolic-local and hyperbolic-stochastic volatility functional forms are considered independently of one another in Sections 2.1.1 and 2.1.2, respectively. The hyperbolic-stochastic volatility function, $g(y)$, is thus ignored in Section 2.1.1 and the hyperbolic-local volatility function, $f(x)$, is ignored in Section 2.1.2.

2.1.1 Hyperbolic-Local Volatility

The hyperbolic-local volatility form presented in (2.3) agrees with the CEV local volatility form, x^β, at $x = 0$ up to the second derivative. It does, however, have certain desirable features that the CEV and DD local volatility forms lack. Specifically, as $x \to 0$, $f(x)$ converges to zero whereas the DD local volatility form does not. As $x \to 0$, $f(x)$ has a finite slope whereas the CEV local volatility form does not. Lastly, as $x \to \infty$, $f(x)$ has a positive slope. As a result of these three features, in the absence of stochasticity of volatility, (2.3) describes the implied volatilities of options with very high and very low strikes as

$$\lim_{k\to 0} \hat{\sigma}_{\text{hyp}}(k) = \frac{\sigma_0}{\beta}$$

and

$$\lim_{k\to \infty} \hat{\sigma}_{\text{hyp}}(k) = \frac{\sigma_0\left(\beta - 1 + \sqrt{1+\beta^2} + \left(1 - \sqrt{1+\beta^2}\right)\right)}{\beta},$$

respectively. The strike is incorporated through $k := K/S_0$.

The feature of $f(x)$ having finite slope near zero is specifically advantageous when it is desirable for the value of the underlying to be strictly positive. As discussed in Chapter 1, having finite slope near zero ensures that the value of x_t does not attain zero, which is allowed for in the CEV and DD models.

2.1.2 Hyperbolic-Stochastic Volatility

Equation 2.4 presents the hyperbolic-stochastic volatility form of the Hyp-Hyp model that is required to maintain accurate scaling of the volatility of volatility (as SABR has). The SABR model can be calibrated to capture volatility distributions ranging from normal to log-normal (although, according to Jäckel and Kahl (2008), the fat tails associated with a log-normal distribution are undesirable). The Hyp-Hyp model should therefore avoid fat tails which are associated with the log-normal distribution while maintaining its desirable properties. The proposed stochastic volatility functional form, $g_{\text{hyp}}(y)$, agrees with the log-normal SABR functional form, attained by $g_{\exp}(y) = e^y$, in its value and first two derivatives at $y = 0$. The third derivative is lower, which results in the slower growth

and decline of $g_{\text{hyp}}(y)$ as $y \to \pm\infty$. This, in turn, results in $g_{\text{hyp}}(y)$ having thinner tails than $g_{\text{exp}}(y)$, while still maintaining the desirable features of the SABR functional form. In fact, the stochastic volatility functional form of the Hyp-Hyp model, $\sigma = \sigma_0\, g(y)$ from (2.1) can be solved along with the expression for $g(y)$, given by (2.4), to yield

$$y = \frac{1}{2}\Big(\frac{\sigma}{\sigma_0} - \frac{\sigma_0}{\sigma}\Big).$$

From this, one can see that as $\sigma \to \infty$, the first term dominates and $\sigma \sim 2\sigma_0 y$, which has the thinner tail of a normal distribution (compared with the log-normal distribution). As $\sigma \to 0$, the second term dominates and $\sigma \sim \frac{-\sigma_0}{2y}$, which is an inverse normal distribution. The inverse normal distribution converges to zero in value and all of its derivatives as $\sigma \to 0$. This is economically desirable as the volatility is suppressed near zero (Jäckel and Kahl, 2008).

2.2 Analytical Approximation for Implied Volatilities

In practice, the model parameters of the Hyp-Hyp model, given by $\Omega_{\text{hyp}-\text{hyp}} = \{\sigma_0, \alpha, \beta, \rho, \kappa\}$, are calibrated to market-observable volatility surfaces for vanilla options. An analytical approximation for Black-Scholes implied volatilities is used for this calibration procedure for numerical tractability. In addition to this, such an approximation will help to better understand the model features such as sensitivities to the various model and option-related parameters.

The analytical approximation was derived by Kahl (2007) using perturbative expansion techniques based on those outlined by Watanabe (1987). A perturbative expansion is used to numerically approximate a solution to an equation using small value expansions. Simply put, this involves the addition of an initially small term to the exact solution of a solvable equation that is similar to the original equation. Similar to the methods used by Kawai (2002) and Osajima (2006), the approximation is derived using Watanabe's expansion in conjunction with an Itô-Taylor expansion of the SDE that describes the process, x_t (that is, (2.1)). Expansions are performed in terms of short maturities and low volatilities but are later extended to longer maturities and higher volatilities. Watanabe's expansion requires, as an input, a decomposition of the SDE in order of decreasing magnitude of noise terms — these are determined using an Itô-Taylor expansion. The resulting implied volatility expression can be thought of as a truncated infinite sum, resulting in an expression,

$$\begin{aligned}\hat{\sigma}(k,T) &= \sum_{i=1}^{\infty} \hat{\sigma}_{i,\text{sl}}(k,T) \\ &\approx \hat{\sigma}_{0,\text{sl}}(k,T) + \hat{\sigma}_{1,\text{sl}}(k,T) + \hat{\sigma}_{2,\text{sl}}(k,T) + \hat{\sigma}_{3,\text{sl}}(k,T) + \hat{\sigma}_{4,\text{sl}}(k,T), \qquad (2.5)\end{aligned}$$

that is applicable for short maturities.

The $\hat{\sigma}_{i,\mathrm{sl}}(k,T)$ terms are described by the model parameters, $\Omega_{\mathrm{hyp-hyp}}$, and option parameters as well as derivatives of $f(x)$ and $g(y)$. The model can be calibrated by observing vanilla option prices, $v(S_0,K,T)$, and calibrating the model parameters, $\Omega_{\mathrm{hyp-hyp}}$, using

$$v(S_0,K,T) = S_0\, B(1,k,\hat{\sigma},T),$$

where $B(F,K,\hat{\sigma},T)$ is the Black-76 formula for the option. The implied volatility, $\hat{\sigma}$, is described by (2.5). The advantage of the stochastic volatility functional form given by (2.4) is that it has $g_3 := g'''(0) = 0$. Higher order derivatives are also zero. This results in the approximation being accurate up to third order deviations of y_t despite it containing only derivatives up to $g_2 := g''(0)$.

As mentioned, (2.5) is derived by using expansions in terms of short maturities. When the implied volatilities from this equation are compared to those given by a Monte Carlo simulation of the SDEs, (2.1) and (2.2), Jäckel and Kahl (2008) found that the analytical approximation gave less accurate implied volatilities for longer times to maturity. Specifically, the estimated implied volatility of longer-dated options tended to be lower than those from a Monte Carlo simulation. An approximation presented by Fouque *et al.* (2000) is more suitable for longer times to maturity. However, the hyperbolic case does not have a closed form solution for the Fouque approximation. Consequently, an approximation that is presented by Kahl (2007) and is similar to the Fouque approximation is used for the Hyp-Hyp model. The analytical approximation for the Hyp-Hyp model can then be scaled to incorporate both longer and shorter times to maturity using the at-the-money (ATM) implied volatilities from the Fouque and Watanabe approximations as follows:

$$\hat{\sigma}_{\mathrm{hyp-hyp}}(k,T) = \hat{\sigma}_{\mathrm{Watanabe}}(k,T)\left(\frac{\hat{\sigma}_{\mathrm{Fouque,ATM}}(T)}{\hat{\sigma}_{\mathrm{Watanabe,ATM}}(T)}(1-h(T)) + h(T)\right). \tag{2.6}$$

The function $h:\mathbb{R}\to[0,1]$ is monotonically decreasing. A more detailed explanation of how (2.6) works is provided in Section 3.3.1. For the Hyp-Hyp model, the most suitable form of h is one that is hyperbolic as it does not decay as fast as an exponential form of h. The equation,

$$h_{\mathrm{hyp-scaling}}(T) = g\Big(-\sqrt{\alpha\kappa T}\Big), \tag{2.7}$$

which is suggested by Kahl (2007), makes use of the hyperbolic function g as defined in (2.4). This is a useful form for h because, for small values of α, the Watanabe expansion is particularly accurate (Jäckel and Kahl, 2008). Thus, for a small α, the function h is not required to approach the Fouque approximation rapidly. Equation 2.7 achieves this by scaling by α.

As mentioned in Section 1.1, the SABR model has time-homogeneous parameters. This is improved in the Hyp-Hyp model by introducing a time-dependent instantaneous volatility, which is specified by allowing for a time-dependent $\sigma_0(t)$ during calibration. Using time-dependent parameters allows the Hyp-Hyp model to be more accurately fitted to observed implied volatility surfaces during calibration. In addition to this, a stochastic volatility inspired (SVI) projection, introduced by Gatheral (2004), corrects the implied volatility from Watanabe's expansion for far-out-the-money options. An SVI projection may be required because Watanabe's expansion contains fourth order polynomial terms of K/F, which lead to inaccuracies for high relative values of K.

The analytical approximation can be used to compute the delta of an option. The computation of the delta has to account for the change in the local volatility parameters (in the function $f(x)$) when the value of S_0 changes. Jäckel and Kahl (2008) derive a generic form of an option delta,

$$\frac{\partial v}{\partial S_0} = B - k\frac{\partial B}{\partial k} + \frac{\partial B}{\partial \hat{\sigma}}\left[\sigma_0(f_1 - 1)\frac{\partial \hat{\sigma}}{\partial \sigma_0} - k\frac{\partial \hat{\sigma}}{\partial k} + \sum_{n=1}^{4}(f_{n+1} + f_n(n - f_1))\frac{\partial \hat{\sigma}}{\partial f_n}\right], \tag{2.8}$$

where $B := B(1, k, \hat{\sigma}, T)$, $f_i = f^{(i)}(1)$ and $\hat{\sigma}$ is defined by (2.5). The partial derivatives can be computed using finite differences.

The analytical approximation is used to calibrate the model using market observable prices as discussed above. Once the model parameters, $\Omega_{\text{hyp}-\text{hyp}}$, are determined, Monte Carlo simulations can be used to price exotic derivatives. When solving the coupled system of SDEs, (2.1) is approximated by a logarithmic Euler-Maruyama scheme that is shown to remain positive by Jäckel and Kahl (2008) for the choice of f given by (2.3) and for $\beta < 1$, which is usually the case after calibration. This is an advantage that this functional form has over the CEV and DD models. Jäckel and Kahl (2008) conclude by illustrating that the approximation given by (2.5) is suitably accurate for approximately at-the-money options. In addition to this, an SVI projection can be used to correct for any deviations in the price of far-out-the-money options, although these options tend to have very low values.

To summarise this section, an analytical approximation for implied volatilities was derived using Watanabe's expansion and Itô-Taylor expansions. A scaling correction was then introduced in order to ensure that the approximation was accurate for longer maturities. More flexibility was added to the model by allowing for the instantaneous volatility to be dependent on time, $\sigma_0(t)$. An SVI projection was mentioned, which corrects the approximation for far out-the-money options. Lastly, an expression for the option delta was derived using the analytical approximation.

Chapter 3

Model Implementation

In this chapter, the Hyp-Hyp model, along with the analytical approximation discussed in Chapter 2, is implemented in various stages and the features of the model are discussed, based on this implementation and previous work done. Firstly, the features of the functional forms given by (2.3) and (2.4) are confirmed. Thereafter, Watanabe's approximation, (2.5), is compared to Fouque's approximation derived by Kahl (2007) along with the scaled combinations of the two approximations. The approximations are also compared to implied volatilities from a Monte Carlo simulation. This chapter also outlines in more detail the work presented by Jäckel and Kahl (2008). Any general statements made in the literature are expanded upon and explained in order to improve understanding of the Hyp-Hyp model. The statements made in Chapter 2 are verified and plots to demonstrate the features of the Hyp-Hyp model are presented. The model is compared to the CEV and SABR models to verify the local and stochastic volatility features, respectively. This is because these are particularly popular local and stochastic volatility models.

Before discussing details of the implementation, it is necessary to perform a change of variables in order to verify initial condition of (2.1). For the SDE describing the value of the underlying, (2.1), Jäckel and Kahl (2008) have assumed that $x_0 = 1$ and that $f(1) = 1$. If the SDE is described as

$$dS_t = \tilde{\sigma}\tilde{f}(S_t)g(y_t)dW_t,$$

with an initial value of S_0, then one can define

$$\sigma_0 := \frac{\tilde{\sigma}\tilde{f}(S_0)}{S_0},$$
$$x_t := \frac{S_t}{S_0}$$

and

$$f(x_t) := \frac{\tilde{f}(x_t S_0)}{\tilde{f}(S_0)}. \tag{3.1}$$

From this arbitrary representation ($\tilde{\sigma}$ and $\tilde{f}$ have not been defined), (2.1) can be obtained from Itô's lemma:

$$\begin{aligned} dx_t &= \frac{1}{S_0} dS_t \\ &= \frac{\sigma_0}{\tilde{\sigma}\tilde{f}(S_0)} \tilde{\sigma}\tilde{f}(S_t) g(y_t) dW_t \\ &= \frac{\sigma_0}{\tilde{\sigma}\frac{\tilde{f}(x_t S_0)}{f(x_t)}} \tilde{\sigma}\tilde{f}(x_t S_0) g(y_t) dW_t \\ &= \sigma_0 f(x_t) g(y_t) dW_t, \end{aligned}$$

with $x_0 = S_0/S_0 = 1$ and $f(1) = \tilde{f}(S_0)/\tilde{f}(S_0) = 1$ as required. As a result of the change of variables given by (3.1), a vanilla call option, with price C_0, struck on S_T can be valued by first valuing the same type of option struck on x_T and then multiplying this price by S_0. This can be seen by considering the discounted risk-neutral expectation of the option payoff,

$$\begin{aligned} C_0 &= e^{-rT}\mathbb{E}_{\mathbb{Q}}[(S_T - K)^+] \\ &= e^{-rT}\mathbb{E}_{\mathbb{Q}}\left[S_0\left(\frac{S_T}{S_0} - \frac{K}{S_0}\right)^+\right] \\ &= S_0 e^{-rT}\mathbb{E}_{\mathbb{Q}}[(x_T - k)^+] =: S_0 c_0, \end{aligned}$$

where $\mathbb{Q}$ is the equivalent risk-neutral measure and c_0 is the value of a call option struck on x_T. The same logic can be applied to the valuation of a vanilla put option.

3.1 Hyperbolic-Local Volatility

As discussed in Section 2.1.1, the hyperbolic-local volatility form presented in (2.3) has certain desirable features over the CEV and DD local volatility functional forms. The functional form of the CEV model, $f_{\text{CEV}}(x) = x^\beta$, and the DD model, $f_{\text{DD}}(x) = \beta x + (1-\beta)x_0$, are plotted along with the hyperbolic-local volatility functional form in Figures 3.1 and 3.2 which show the features mentioned in Section 2.1.1.

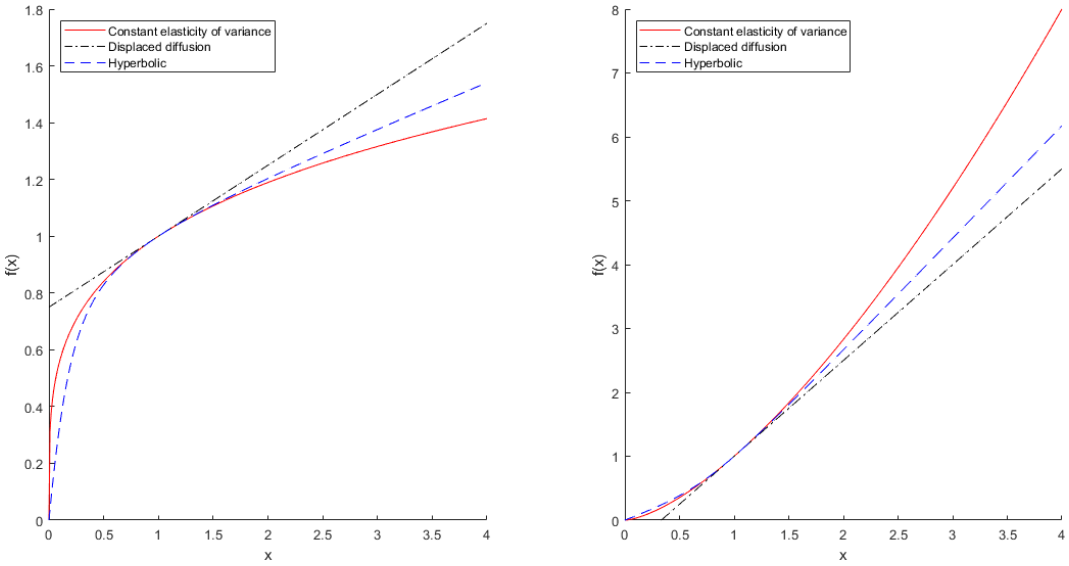

Fig. 3.1: Local volatility for the CEV (red, solid), DD (black, dash-dot) and hyperbolic (blue, dash) functional forms for $\beta = 1/4$ (left) and $\beta = 3/2$ (right).

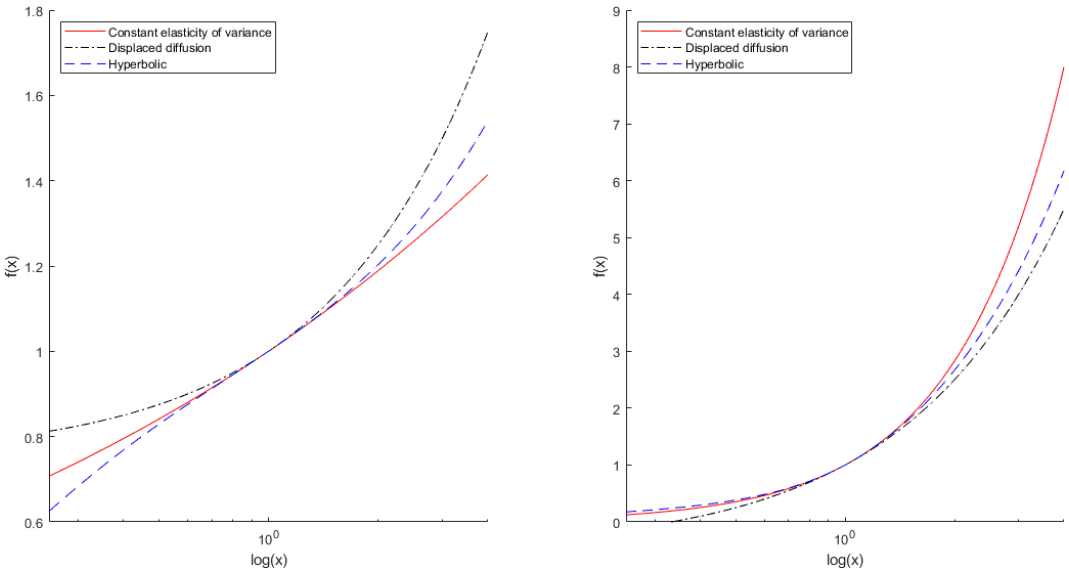

Fig. 3.2: Local volatility for the CEV (red, solid), DD (black, dash-dot) and hyperbolic (blue, dash) functional forms for $\beta = 1/4$ (left) and $\beta = 3/2$ (right) plotted on a logarithmic scale.

Firstly, as $x \to 0$, one can see that the CEV functional form, $f_{\text{CEV}}(x) \to 0$ and that its slope $f'_{\text{CEV}}(x) = \beta \frac{x^\beta}{x} \to \infty$ for $\beta < 1$ (for example, $\beta = 1/4$ above). For the DD functional form, the function value $f_{\text{DD}}(x) \to (1-\beta)x_0$ and the slope $f'_{\text{DD}}(x) = \beta \to \beta$ as $x \to 0$. As $x \to 0$, the functional form given by (2.3), denoted by $f_{\text{hyp}}(x)$,

approaches

$$f_{\text{hyp}}(x) \to \frac{\sqrt{\beta^2} - \beta}{\beta} = 0,$$

while the slope is given by

$$f'_{\text{hyp}}(x) = \frac{(1 - \beta + \beta^2)}{\beta} + \frac{\beta - 1}{\beta} \frac{(x - \beta^2 + \beta^2 x)}{\sqrt{x^2 + \beta^2(1-x)^2}} \tag{3.2}$$

and approaches

$$f'_{\text{hyp}}(x) \to \frac{(1 - \beta + \beta^2)}{\beta} - \beta + 1 = \frac{1}{\beta}.$$

From this, it can be seen that the hyperbolic-local volatility functional form has a finite slope as $x \to 0$ which is deemed a desirable feature by Jäckel and Kahl (2008) as it ensures that the value of the underlying asset, x_t, does not attain or drop below zero. In this way, the Hyp-Hyp model has an advantage over a model with a CEV local volatility functional form. In addition, the suppression of volatility near zero (that is, $f(x) \to 0$ as $x \to 0$) is also deemed desirable. The suppression of volatility is therefore a desirable feature that the Hyp-Hyp model has over a model with a DD local volatility functional form.

The functional form given by (2.3) agrees with the CEV functional form up to its second order derivative at the initial conditions. The initial value of $f_{\text{hyp}}(1) = 1$ is in agreement with that of the CEV functional form: $f_{\text{CEV}}(1) = 1^\beta = 1$. Equation 3.2 gives the first derivative and it can be shown from this that $f'_{\text{hyp}}(1) = \beta$, which is identical to $f'_{\text{CEV}}(1) = \beta$. The second order derivative of the CEV functional form is $f''_{\text{CEV}}(x) = \beta(\beta - 1)x^{\beta-2}$ and thus $f''_{\text{CEV}}(1) = \beta(\beta - 1)$. The second derivative of the hyperbolic-local volatility functional form,

$$f''_{\text{hyp}}(x) = \frac{\beta - 1}{\beta}\left[\frac{1 + \beta^2}{\sqrt{x^2 + \beta^2(1-x)^2}} - \frac{(x - \beta^2 + \beta^2 x)^2}{\left(x^2 + \beta^2(1-x^2)^2\right)^{3/2}}\right], \tag{3.3}$$

agrees with this. That is, $f''_{\text{hyp}}(1) = \beta(\beta - 1)$.

Another advantage that, according to Jäckel and Kahl (2008), the Hyp-Hyp model has over the CEV model is that it has a finite slope as $x \to \infty$. Depending on the value of β, the CEV model has either an infinite slope or a slope of 0 (both of which can be seen in Figure 3.1). As $x \to \infty$, the CEV functional form $f'_{\text{CEV}}(x) = \beta\frac{x^\beta}{x} \to \infty$ if $\beta > 1$ and $f'_{\text{CEV}}(x) \to 0$ if $\beta < 1$. However, for the Hyp-

Hyp model, it can be seen that, as $x \to \infty$,

$$\begin{aligned}\lim_{x\to\infty} \frac{x - \beta^2 + \beta^2 x}{\sqrt{x^2 + \beta^2(1-x)^2}} &= \lim_{x\to\infty} \frac{\frac{1}{x}(x - \beta^2 + \beta^2 x)}{\frac{1}{x}(\sqrt{x^2 + \beta^2(1-x)^2})} \\ &= \lim_{x\to\infty} \frac{1 - \frac{\beta^2}{x} + \beta^2}{\sqrt{1 + \frac{\beta^2}{x^2} - \frac{2\beta^2}{x} + \beta^2}} \\ &= \sqrt{1+\beta^2},\end{aligned}$$

which means that, as $x \to \infty$,

$$f'_{\text{hyp}}(x) \to \frac{1 - \beta + \beta^2 + (\beta - 1)\sqrt{1+\beta^2}}{\beta},$$

which is finite as desired.

3.2 Hyperbolic-Stochastic Volatility

This section provides an introduction to various stochastic volatility functions that are compared to one another. First, the functions themselves will be discussed. Second, the densities of the functions will be compared to one another. In order to compare the densities of the functions, the density of the volatility driver is determined and transformations of this density (based on the functional form) are performed. Finally, the densities will be analysed and the advantageous features of the hyperbolic-stochastic volatility function will be discussed.

The hyperbolic-stochastic volatility is written as a function of a normally distributed volatility driver, y_t, in (2.4). The function is henceforth referred to as $g_{\text{hyp}}(y)$. Similarly, the SABR stochastic volatility can be written as an exponential function of the volatility driver: $g_{\exp}(y) = e^y$. This can be seen by considering the SABR model SDEs,

$$dx_t = x_t \sigma_t dW_t$$

and

$$d\sigma_t = \alpha_{\text{SABR}} \sigma_t dZ_t, \tag{3.4}$$

where α_{SABR} is different to α in the Hyp-Hyp model and σ_t is the stochastic volatility. The solution to (3.4) implies that σ_t is log-normally distributed. The SABR stochastic volatility function can therefore be written as $g_{\exp}(y_t) := \sigma_t = e^{y_t}$. In addition, an affine functional form $g_{\text{aff}}(y) = y + 1$ is also compared with $g_{\text{hyp}}(y)$ in Figure 3.3.

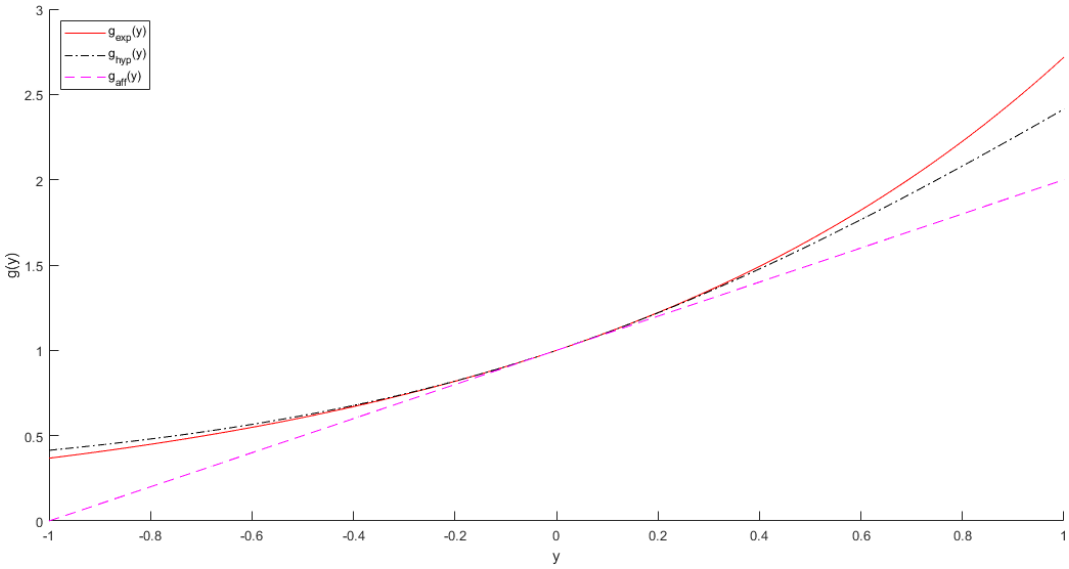

Fig. 3.3: The exponential (red, solid), hyperbolic (black, dash-dot) and affine (pink, dash) stochastic volatility functional forms.

As can be seen in Figure 3.3, $g_{\text{hyp}}(y)$ is identical in value with $g_{\exp}(y)$ at $y = 0$. It is, however, also identical in the first two derivatives at $y = 0$. Trivially, $g'_{\exp}(0) = g''_{\exp}(0) = 1$. One can see that

$$g'_{\text{hyp}}(y) = 1 + \frac{y}{\sqrt{y^2+1}}$$

and

$$g''_{\text{hyp}}(y) = \frac{1}{\sqrt{y^2+1}} - \frac{y^2}{(y^2+1)^{3/2}}.$$

These functions agree with $g_{\exp}(y)$ at $y = 0$. However, $g_{\text{hyp}}(y)$ has a lower third order,

$$g'''_{\text{hyp}}(y) = \frac{-3y}{(y^2+1)^{3/2}} + \frac{3y^3}{(y^2+1)^{5/2}},$$

and higher order derivatives than $g_{\exp}(y)$. The third order derivative evaluates to $g'''_{\text{hyp}}(0) = 0$. This feature results in $g_{\text{hyp}}(y)$ increasing less rapidly as $y \to \infty$ and decreasing less rapidly as $y \to -\infty$ than $g_{\exp}(y)$. The consequence of this can be analysed by considering the densities of each of the above functional forms that are presented in Figure 3.4.

In order to compute the densities of these various functional forms, the density of the volatility driver, y_t needs to first be considered. The dynamics of y_t are described by (2.2). This is an Ornstein-Uhlenbeck process and can be solved using an integrating factor. The SDE is given by

$$dy_t = -\kappa y_t dt + \alpha\sqrt{2\kappa} dZ_t,$$

and has the solution

$$y_T e^{\kappa T} = y_0 e^{\kappa(0)} + \int_0^T e^{\kappa t}\alpha\sqrt{2\kappa}dZ_t.$$

Because $y_0 = 0$, one can see that

$$y_T = \alpha\sqrt{2\kappa}\int_0^T e^{-\kappa(T-t)}dZ_t,$$

which implies, by Itô isometry, that

$$y_T \sim \mathcal{N}\Big(0, 2\kappa\alpha^2\int_0^T e^{-2\kappa(T-t)}dt\Big). \tag{3.5}$$

Computing this integral, one arrives at the distribution of the volatility driver being $y_t \sim \mathcal{N}\Big(0, \eta^2\Big)$ where $\eta := \alpha\sqrt{1-e^{-2\kappa T}}$. If the instantaneous volatility from (2.1) is defined as $\sigma_t = \sigma_0 g(y_t)$, then the density of σ_t (denoted as σ for practical purposes) can be determined from the density of y_t (denoted as y for these purposes). For $g_{\exp}(y)$,

$$\begin{aligned}\sigma = \sigma_0 e^y \implies \log\sigma &= y + \log\sigma_0\\ \implies \log\sigma &\sim \mathcal{N}\Big(\log\sigma_0, \eta^2\Big).\end{aligned}$$

That is, σ is log-normally distributed for the SABR functional form $g_{\exp}(y)$ (as briefly mentioned above). A similar approach can be used to show that a functional form of $g_{\text{aff}}(y)$ implies that $\sigma \sim \mathcal{N}(\sigma_0, \eta^2\sigma_0^2)$. For the functional form, $g_{\text{hyp}}(y)$, one has to be a more careful. The function $h(y)$ is defined as

$$\sigma = \sigma_0 g_{\text{hyp}}(y) = \sigma_0\big(y + \sqrt{y^2+1}\big) =: h(y).$$

Inverting this results in

$$y = h^{-1}(\sigma) = \frac{1}{2}\Big(\frac{\sigma}{\sigma_0} - \frac{\sigma_0}{\sigma}\Big). \tag{3.6}$$

In order to transform the probability density function of y to that of σ, it is necessary to define the cumulative distribution function of σ:

$$\begin{aligned}F_\sigma(x) &= \mathbb{P}\big[\sigma \le x\big]\\ &= \mathbb{P}\big[h(y) \le x\big]\\ &= \mathbb{P}\big[y \le h^{-1}(x)\big]\\ &= F_y\big(h^{-1}(x)\big).\end{aligned}$$

Differentiating both sides, one arrives at

$$f_\sigma(x) = f_y\big(h^{-1}(x)\big)\frac{\partial h^{-1}(x)}{\partial x}, \tag{3.7}$$

where $f_y(x)$ is the probability density function of y that is normally distributed with mean 0 and variance η^2. Differentiating (3.6) results in

$$\frac{\partial h^{-1}(\sigma)}{\partial \sigma} = \frac{1}{2\sigma_0} + \frac{\sigma_0}{2\sigma^2}.$$

By substituting this, along with the probability density function for the normal distribution, (3.8) can be written as

$$f_\sigma(x) = \frac{1}{\sqrt{2\pi\eta^2}} e^{-\frac{\left(\frac{x}{\sigma_0} - \frac{\sigma_0}{x}\right)^2}{8\eta^2}} \left[\frac{1}{2\sigma_0} + \frac{\sigma_0}{2x^2}\right]. \tag{3.8}$$

This density function is plotted in Figure 3.4 and compared with the log-normal density in order to verify its desirable features.

In Jäckel and Kahl (2008), a CIR process is fitted to the hyperbolic density and we replicate this result. The CIR process,

$$dv_t = \kappa_{\text{CIR}}(\theta_{\text{CIR}} - v_t)dt + \alpha_{\text{CIR}}\sqrt{v_t}dZ_t,$$

where $v_t = \sigma^2$ and CIR parameters,

$$\Omega_{\text{CIR}} = \{v_0, \alpha_{\text{CIR}}, \kappa_{\text{CIR}}, \theta_{\text{CIR}}\} = \{0.0625, 0.250847, 0.389852, 0.098938\},$$

is found to fit the hyperbolic density (Jäckel and Kahl, 2008). The CIR subscript will be dropped for the purposes of this explanation but α, κ and θ are still the CIR parameters defined above. According to Vanyolos *et al.* (2014), the probability density function of a CIR process is given by

$$f_{v_t}(v_t; v_0, \alpha, \kappa, \theta) = ce^{-u-v}\left(\frac{v}{u}\right)^{q/2} I_q(2\sqrt{uv}), \tag{3.9}$$

where $q = \frac{2\kappa\theta}{\sigma^2} - 1$, $c = \frac{2\kappa}{(1-e^{-\kappa t})}$, $u = cv_0e^{-\kappa t}$ and $v = cv_t$. In addition, $I_\nu(x)$ is a modified Bessel function of the first kind,

$$I_\nu(x) = \sum_{k=0}^{\infty} \frac{\left(\frac{z}{2}\right)^{2k+\nu}}{k!\Gamma(\nu + k + 1)}.$$

Now, σ is a function of v_t: $\sigma = \sqrt{v_t}$. Thus, performing a similar probability density function transformation as that done to derive (3.7), one can obtain

$$f_\sigma(x) = 2\sigma f_{v_t}(v_t; v_0, \alpha, \kappa, \theta). \tag{3.10}$$

Plotting the density of the instantaneous volatility, σ, based on $g_{\text{exp}}(y)$, $g_{\text{aff}}(y)$, $g_{\text{hyp}}(y)$ and the fitted CIR process, results in Figure 3.4.

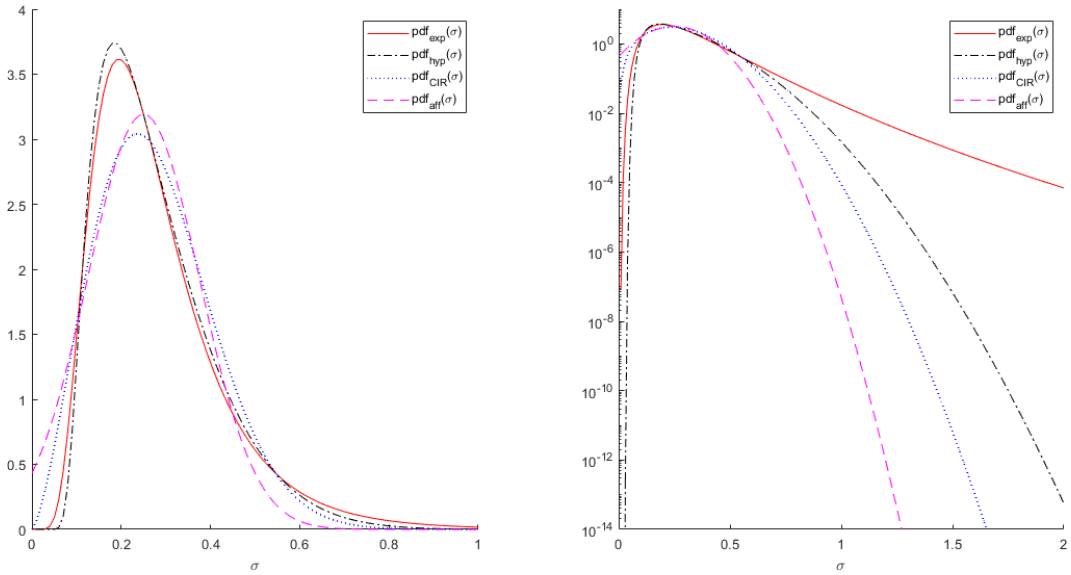

Fig. 3.4: Probability density functions of the exponential (red, solid), hyperbolic (black, dash-dot) and affine (pink, dash) transformations of the driving Ornstein-Uhlenbeck process, $\sigma = \sigma_0 g(y)$, plus the density of fitted CIR process (blue, dot). The parameters used were: $\sigma_0 = 25\%$, $\kappa = 1/2$, $T = 5$ and $\eta = 1/2$. The same densities are plotted on a logarithmic scale on the right.

From Figure 3.4, one can see the features that were briefly mentioned in Section 2.1.2. The affine stochastic volatility functional form, $g_{\text{aff}}(y)$, results in a normally distributed σ while the exponential form, $g_{\text{exp}}(y)$ results in a log-normally distributed σ. It can be seen in the first plot that the normally distributed σ has thinner tails than its log-normal counterpart, which, as discussed in Section 2.1.2, is desirable. However, the density of the normally distributed σ does not converge to zero as σ approaches zero. Jäckel and Kahl (2008) deem this a desirable feature, as mentioned in Section 2.1.2, because it ensures that the value of the underlying, x_t, does not attain or drop below zero (via Equation 2.1). It can be seen in the figure that the density of the log-normal σ does have this desirable feature. Figure 3.4 clearly shows that the $g_{\text{hyp}}(y)$ and the fitted CIR process have densities that approach zero as σ approaches zero while also having thinner tails than the log-normal distribution corresponding to the $g_{\text{exp}}(y)$ transformation. They therefore have the desirable features of both the $g_{\text{aff}}(y)$ and $g_{\text{exp}}(y)$ while avoiding the undesirable features. The discussion presented in Section 2.1.2 provides an explanation as to why this is so for the $g_{\text{hyp}}(y)$ transformation.

3.3 Analytical Approximation

Approximations derived by Kahl (2007) based on Watanabe and Fouque's approximations are presented in this section. The detailed derivations of these approximations are outlined in Appendix A. The Fouque approximation presented in this section differs from that used by Jäckel and Kahl (2008) as it incorporates the two corrections made to the Fouque approximation in Appendix A.1.

3.3.1 Approximations and Scaling Corrections

A major second achievement of the work presented in Jäckel and Kahl (2008) is an analytical approximation for implied volatility. The expansion is given by (2.5),

$$\hat{\sigma}(k,T) \approx \hat{\sigma}_{0,\mathrm{sl}}(k,T) + \hat{\sigma}_{1,\mathrm{sl}}(k,T) + \hat{\sigma}_{2,\mathrm{sl}}(k,T) + \hat{\sigma}_{3,\mathrm{sl}}(k,T) + \hat{\sigma}_{4,\mathrm{sl}}(k,T),$$

and the $\hat{\sigma}_{i,\mathrm{sl}}(k,T)$ terms are defined as

$$\hat{\sigma}_{1,\mathrm{sl}} = \frac{\sigma_0 z}{2\sqrt{T}}\left((f_1-1)\sigma_0 T + \sqrt{8}g_1\alpha\rho\frac{(\kappa T + e^{\kappa T} - 1)}{T\kappa^{3/2}}\right),$$

$$\begin{aligned}
\hat{\sigma}_{2,\mathrm{sl}} = \sigma_0\frac{e^{-2T\kappa}}{24T^3\kappa^3}\Bigg[&12\sqrt{2}e^{T\kappa}f_1 g_1\alpha\kappa^{3/2}(e^{T\kappa}(T\kappa-1)+1)\rho\sigma_0 T^2 \\
&- T\kappa\Big[e^{2T\kappa}(f_1^2-2f_2-1)T^3\kappa^2\sigma_0^2 \\
&\quad - 6g_2\alpha^2(2e^{2T\kappa}T^2\kappa^2 - 5e^{2T\kappa}T\kappa + T\kappa - 8e^{T\kappa} + 6e^{2T\kappa})\rho^2\Big] \\
&\quad - 6g_1^2\alpha^2\Big[\big(2e^{2T\kappa}T^3\kappa^3(\rho^2-1) + (-9\rho^2e^{2T\kappa} + \rho^2 + 5e^{2T\kappa} - 1)T^2\kappa^2 \\
&\qquad - 2(e^{T\kappa}-1)(-7\rho^2e^{T\kappa} + \rho^2 + 3e^{T\kappa} - 1)T\kappa - 4\rho^2(e^{\kappa T}-1)^2\big)\Big] \\
&+ z^2\Big[-12\sqrt{2}e^{T\kappa}g_1\alpha\kappa^{3/2}(e^{T\kappa}(T\kappa-1)+1)\rho\sigma_0 T^2 \\
&\quad - T\kappa\Big[e^{2T\kappa}(2f_1^2+6f_1-4f_2-8)T^3\kappa^2\sigma_0^2 \\
&\qquad - 6g_2\alpha^2(4e^{2T\kappa}T\kappa + 8e^{T\kappa} - 6e^{2T\kappa} - 2)\rho^2\Big] \\
&\qquad - 6g_1^2\alpha^2\Big[(12\rho^2e^{2T\kappa} - 4e^{2T\kappa})T^2\kappa^2 + 8\rho^2(e^{\kappa T}-1)^2 \\
&\qquad\quad - 2(e^{T\kappa}-1)(11\rho^2e^{T\kappa} - \rho^2 - 3e^{T\kappa} + 1)T\kappa\Big]\Big]\Bigg],
\end{aligned}$$

$$\begin{aligned}
\hat{\sigma}_{3,\mathrm{sl}} = \frac{T^{3/2}z\sigma_0^4}{48}\Bigg[&-f_1^3 + f_1^2 + (2f_2+3)f_1 - 2f_2 + 2f_3 - 3 \\
&+ 2z^2\Big[f_1^3 + f_1^2 + (4-2f_2)f_1 - 2f_2 + f_3 - 6\Big]\Bigg],
\end{aligned}$$

$$\begin{aligned}\hat{\sigma}_{4,\text{sl}} = -\frac{T^2\sigma_0^5}{5760}\Bigg[&8z^4\Big[19f_1^4+15f_1^3+(20-46f_2)f_1^2+6(3f_3-5f_2+15)f_1\\&40f_2+(16f_2^2+15f_3)-6f_4-144\Big]\\&-2z^2\Big[11f_1^4+30f_1^3+(20-44f_2)f_1^2+6(12f_3-10f_2-45)f_1\\&+140f_2+(44f_2^2-60f_3)+36f_4+209\Big]\\&-3\Big[3f_1^4-2(6f_2+5)f_1^2+16f_3f_1+12f_2^2+20f_2+8f_4+7\Big]\Bigg],\end{aligned}$$

where $z := (k-1)/(\sigma_0\sqrt{T})$. A detailed derivation of these terms is given in Section A.2.

As discussed in Section 2.2, the approximation is based on a Watanabe expansion but is scaled along with an approximation based on work done by Fouque *et al.* (2000).

The Watanabe approximation, (2.5), contains terms that are functions of the model and option parameters, $\Omega_{\text{hyp}-\text{hyp}}$, k, T and various higher order derivatives of (2.3) and (2.4). If one defines $f_i = f^{(i)}(1)$ and $g_i = g^{(i)}(0)$, it has been shown that $f_1 = \beta$ and $f_2 = \beta(\beta-1)$ and that $g_1 = g_2 = 1$. It can also be shown that $f_3 = -3\beta(\beta-1)$ and $f_4 = -3\beta(\beta-1)(\beta^2-4)$.

The Fouque approximation, which is introduced in Section 2.2, given by

$$\begin{aligned}\hat{\sigma}_{\text{Fouque}} =&\sigma_0\sqrt{\frac{(-1+e^{-2\kappa T})\alpha^2}{T\kappa}+2\alpha^2+1}-\frac{\alpha(-4\alpha^6+\alpha^4-3\alpha^2-1)\rho\sigma_0^2}{\sqrt{2\Big(\frac{(-1+e^{-2\kappa T})\alpha^2}{T\kappa}+2\alpha^2+1\Big)\kappa}}\\&-\frac{\sqrt{2T}\alpha(-4\alpha^6+\alpha^4-3\alpha^2-1)\kappa\rho}{\Big((2T\kappa+e^{-2T\kappa}-1)\alpha^2+T\kappa\Big)^{3/2}}\ln\Big(\frac{K}{F}\Big),\end{aligned}\tag{3.11}$$

is scaled along with the Watanabe approximation using the scaling formula, (2.6). The scaling formula, reproduced here for convenience,

$$\hat{\sigma}_{\text{hyp}-\text{hyp}}(k,T) = \hat{\sigma}_{\text{Watanabe}}(k,T)\left(\frac{\hat{\sigma}_{\text{Fouque,ATM}}(T)}{\hat{\sigma}_{\text{Watanabe,ATM}}(T)}(1-h(T))+h(T)\right),$$

adjusts Watanabe's approximation based on maturity by introducing a maturity-dependent shift. The equation can be seen as Watanabe's approximation being multiplied by a term (the entire bracketed term) which is only a function of T. The term makes use of the ratio of Watanabe's and Fouque's approximations for an at-the-money option as this is the region in which both of these approximations are the most accurate. The formula becomes a strict convex combination of Watanabe's and Fouque's approximation for an at-the-money option.

The hyperbolic scaling function given by (2.7),

$$h_{\text{hyp}-\text{scaling}}(T) = g\Big(-\sqrt{\alpha\kappa T}\Big),$$

was found to be more effective than the exponential scaling form,

$$h_{\text{exp}-\text{scaling}(1)}(T) = e^{-\kappa T}, \tag{3.12}$$

while a second exponential scaling function,

$$h_{\text{exp}-\text{scaling}(2)}(T) = e^{-\sqrt{\alpha\kappa T}}, \tag{3.13}$$

is also more appropriate. As mentioned in Section 2.2, the hyperbolic scaling function, (2.7), is useful because the Watanabe expansion is more accurate, and should thus be weighted more heavily, for small values of α. For this reason, (3.13) is expected to be more accurate than (3.12).

3.3.2 Monte Carlo

A Monte Carlo simulation of (2.1) and (2.2) was used to assess the accuracy of the various approximations. Firstly, the simulation of the SDE given by (2.2) is considered. As shown in Section 3.2, the distribution of y_t,

$$\begin{aligned} y_t &\sim \mathcal{N}\Big(y_0 e^{-\kappa t}, 2\kappa\alpha^2 \int_0^t e^{-2\kappa(t-u)} du\Big) \\ \implies y_t &\sim \mathcal{N}\Big(y_0 e^{-\kappa t}, \alpha^2(1-e^{-2\kappa t})\Big), \end{aligned} \tag{3.14}$$

is the solution to the Ornstein-Uhlenbeck process describing y_t. According to Finch (2004), an Ornstein-Uhlenbeck process can be defined recursively as

$$y_{t_{n+1}} = \mu_n + \kappa_n(y_{t_n} - \mu_n) + \sqrt{1-\kappa_n^2}\alpha Z_n, \tag{3.15}$$

where $\mu_n = \mathbb{E}[y_{t_n}] = y_0 e^{-\kappa t_n}$ (from (3.14)), $\kappa_n = e^{-\frac{\kappa t_n}{n}}$ and Z_n is a normal random number. The reason that the Ornstein-Uhlenbeck process needs to be defined recursively is that the correlation between the Brownian motion driving y_t and that driving x_t, ρ, needs to be incorporated at every time step.

The logarithmic solution of the SDE given by (2.1) is given by

$$\ln x_t = \ln x_0 - \frac{1}{2}\sigma_0^2 \int_0^t \left(\frac{f(x_u)}{x_u} g(y_u)\right)^2 du + \sigma_0 \int_0^t \left(\frac{f(x_u)}{x_u} g(y_u)\right) dW_u.$$

A logarithmic Euler-Maruyama approximation scheme,

$$\ln x_{t_{n+1}} = \ln x_{t_n} - \frac{1}{2}\sigma_0^2 \left(\frac{f(x_{t_n})}{x_{t_n}} g(y_{t_n})\right)^2 \Delta t_n + \sigma_0 \left(\frac{f(x_{t_n})}{x_{t_n}} g(y_{t_n})\right) \Delta W_n, \tag{3.16}$$

is suggested by Jäckel and Kahl (2008) for the discretised simulation of the SDE (2.1). In (3.16), ΔW_n is a Brownian increment distributed as $\Delta W_n \sim \mathcal{N}(0, \Delta t_n)$.

We make use of (3.15) and (3.16) in order to simulate the values of the underlying, x_t, and the volatility driver, y_t, at various time steps. The value of x_t needs to be updated with the previous value of both x_t and y_t, which is why this joint simulation needs to be done. Once the value of the underlying at maturity, x_T, is simulated in this way, the value of a call option can be computed as the risk-neutral expectation of the discounted payoff:

$$c_0 = \mathbb{E}_{\mathbb{Q}}[e^{-rT}(x_T - K)^+] = \mathbb{E}_{\mathbb{Q}}[(x_T - K)^+],$$

where $r = 0$ because x_T is the forward value of the underlying. The estimator for the value of the call option is therefore

$$\hat{c}_{0,n} := \frac{1}{n}\sum_{i=1}^{n}(x_T^{(i)} - K)^+,$$

where $x_T^{(1)}, ..., x_T^{(n)}$ are the n sample values of the underlying. The implied volatility is then determined by solving for the $\hat{\sigma}$ that recovers the simulated c_0 using the Black-76 formula mentioned in Section 2.2.

3.3.3 At-the-money Implied Volatility

The results of the Monte Carlo are compared to the implied volatilities recovered from the Watanabe and Fouque approximations (and the various scalings thereof) for various maturities. The implied volatilities are presented for at-the-money European call options in Figure 3.5.

As can be seen in these plots, both Equations 2.7 (orange diamonds) and 3.13 (yellow squares) match the implied volatility of the Monte Carlo simulation reasonably closely with (2.7) perhaps matching it slightly better. It can also be seen that the Fouque approximation tends to overestimate the implied volatility while the Watanabe approximation tends to underestimate the implied volatility. Lastly, the scaling given by (3.12) can be seen to match the Monte Carlo implied volatility poorly compared with the other two scaling functions.

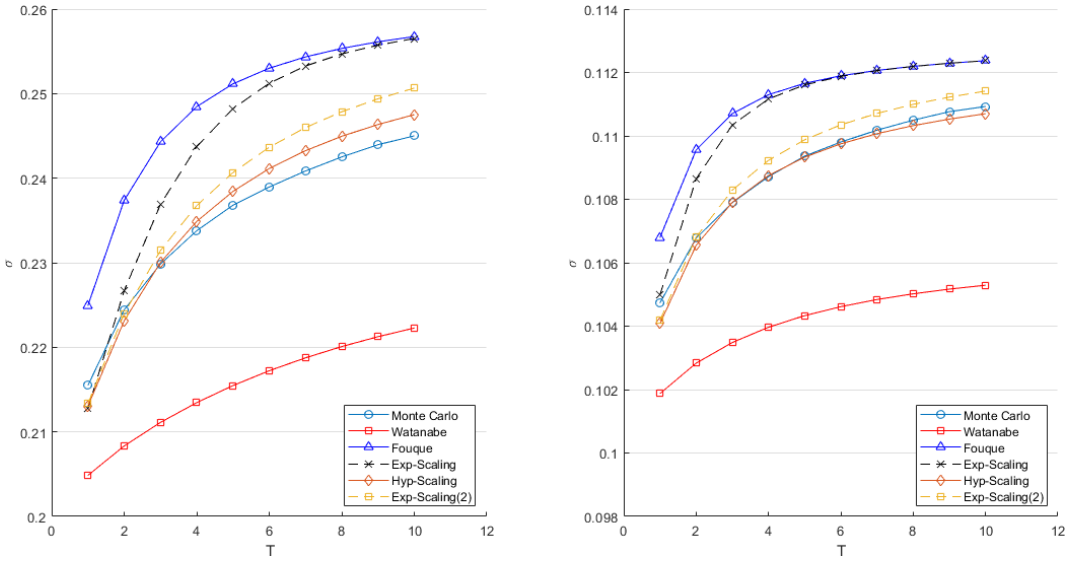

Fig. 3.5: Implied volatilities for an at-the-money option using the Fouque and Watanabe approximations (and the different scalings thereof) compared to a Monte Carlo simulation using (3.15) and (3.16). The parameters for each of the plots are: $\alpha = 3/5$, $\beta = 1$, $\kappa = 1/2$, $\sigma_0 = 1/5$ and $\rho = 0$ (left); $\alpha = 2/5$, $\beta = 1$, $\kappa = 1$, $\sigma_0 = 1/10$ and $\rho = -1/2$ (right). The Monte Carlo used a stepsize of $\Delta t = 1/16$ and $N = 2^{22} - 1$ sample paths.

While the left hand plot of Figure 3.5 is identical to the result presented by Jäckel and Kahl (2008), the right hand plot differs slightly. Firstly, in order to obtain both plots for the Fouque approximation in Figure 3.5, the expression given by (3.11) is used. This expression differs slightly from the result given by both Jäckel and Kahl (2008) and Kahl (2007) and presents a correction to these expressions. As mentioned above, the correction does not significantly change the result in Figure 3.5. The detailed derivation of this expression is given in Appendix A.1. Secondly, the Watanabe approximation in 3.5 is shifted slightly up when compared with the identical plot in Jäckel and Kahl (2008). As shown in Appendix A.2, the expression for Watanabe's approximation given by Jäckel and Kahl (2008) is recovered from the detailed derivation. The shift of this approximation may be as a result of a different implementation of the approximation. It is important to note, however, that two independent and different implementations of the expression given by (2.5) as detailed at the beginning of Section 3.3 result in the plot presented on the right hand side of Figure 3.5. The first implementation makes use of the approximation described by (2.5) directly while the second implementation uses the simplest expressions for the terms in (A.20) in Appendix A.2. It is also important to note that the upward shift of Watanabe's approximation in this plot results in

an upper shift of all of the scaled approximations. This shift in the hyperbolically scaled approximation results in it being very close to the Monte Carlo plot.

The plots of implied volatility as a function of maturity for at-the-money options is presented here first in order to first investigate the scaled approximation for at-the-money options. Next, an expression for the delta of an option (which is a byproduct of the analytical approximation) is presented. The effect that a changing strike will have on the implied volatility (that is, the volatility smile) is then discussed in Section 3.3.5.

3.3.4 Delta

A by-product of the analytical approximation presented by Jäckel and Kahl (2008) is an expression for the delta of an option. Equation 2.8 gives the expression for the delta of an option based on Watanabe's expansion, (2.5). Because there is a closed-form solution for delta given DD functional forms, these functional forms will be plotted. The derived delta sensitivity can thus be compared to a closed-form solution. However, the expression will still be applicable to the hyperbolic functional forms and the delta for the Hyp-Hyp model can be computed in an identical way using the hyperbolic functions, (2.3) and (2.4). For the DD model, the higher order derivative terms are

$$\begin{aligned} &f_1^{\mathrm{DD}} = \beta, \qquad f_2^{\mathrm{DD}} = f_3^{\mathrm{DD}} = f_4^{\mathrm{DD}} = f_5^{\mathrm{DD}} = 0, \\ &g_1^{\mathrm{DD}} = g_2^{\mathrm{DD}} = 0, \end{aligned} \tag{3.17}$$

and $f^{\mathrm{DD}}(x) = \beta x + (1-\beta)x_0$ and $g^{\mathrm{DD}}(y) = 1$. According to Jäckel and Kahl (2008), for the DD model, the exact value of a call option is given by

$$v^{\mathrm{DD}} = B(x_0 + X, K + X, \beta\sigma_0, T),$$

where, as before, $B(F, K, \hat{\sigma}, T)$ is the Black-76 formula for the option and $X = (1-\beta)x_0/\beta$. The exact $\hat{\sigma}$ is determined by solving for $\hat{\sigma}$ in

$$v^{\mathrm{DD}} = B(x_0, K, \hat{\sigma}, T) \tag{3.18}$$

for various values of K. These implied volatilities are compared to the implied volatilities computed using Watanabe's approximation in the right hand plot of Figure 3.6.

The delta expression presented by Jäckel and Kahl (2008) is given by (2.8),

$$\frac{\partial v}{\partial S_0} = B - k\frac{\partial B}{\partial k} + \frac{\partial B}{\partial \hat{\sigma}}\left[\sigma_0(f_1 - 1)\frac{\partial \hat{\sigma}}{\partial \sigma_0} - k\frac{\partial \hat{\sigma}}{\partial k} + \sum_{n=1}^{4}(f_{n+1} + f_n(n - f_1))\frac{\partial \hat{\sigma}}{\partial f_n}\right],$$

where $B := B(1, k, \hat{\sigma}, T)$. The Watanabe function for $\hat{\sigma}$, the model parameters and the functions given in (3.17) are used to compute the delta of an option using (2.8). In order to evaluate the partial derivatives, $\frac{\partial \hat{\sigma}}{\partial k}$, $\frac{\partial \hat{\sigma}}{\partial \sigma_0}$ and $\frac{\partial \hat{\sigma}}{\partial f_i}$ (for $i = 1, 2, 3, 4$), central finite differencing is used. The approximations are

$$\frac{\partial \hat{\sigma}}{\partial k} \approx \frac{\hat{\sigma}(k+h, T, \sigma_0, f_i) - \hat{\sigma}(k-h, T, \sigma_0, f_i)}{2h},$$
$$\frac{\partial \hat{\sigma}}{\partial \sigma_0} \approx \frac{\hat{\sigma}(k, T, \sigma_0+h, f_i) - \hat{\sigma}(k, T, \sigma_0-h, f_i)}{2h}$$

and

$$\frac{\partial \hat{\sigma}}{\partial f_i} \approx \frac{\hat{\sigma}(k, T, \sigma_0, f_i+h) - \hat{\sigma}(k, T, \sigma_0, f_i-h)}{2h},$$

where $\hat{\sigma}(k, T, \sigma_0, f_i)$ is the Watanabe expansion, (2.5), written as a function of only the variables of interest. Similarly, the partial derivatives, $\frac{\partial B}{\partial k}$ and $\frac{\partial B}{\partial \hat{\sigma}}$, are evaluated using the central finite differences,

$$\frac{\partial B}{\partial k} \approx \frac{B(x_0, (k+h)x_0, \hat{\sigma}, T) - B(x_0, (k-h)x_0, \hat{\sigma}, T)}{2h},$$

and

$$\frac{\partial B}{\partial \hat{\sigma}} \approx \frac{B(x_0, K, \hat{\sigma}+h, T) - B(x_0, K, \hat{\sigma}-h, T)}{2h}.$$

The exact call option delta (given by the closed form solution for the delta of the DD model) ,

$$\Delta^{\mathrm{DD}} = \Phi\left(\ln\left(\frac{S+X}{K+X}\right) / (\beta\sigma_0\sqrt{T}) + \beta\sigma_0\sqrt{T}/2 \right),$$

is plotted with the delta computed using (2.8) in the right hand plot of Figure 3.6.

In the figure, the approximate Black delta is computed using Black's formula for delta and the $\hat{\sigma}$'s computed using Watanabe's approximation. The at-the-money Black delta is computed using σ_0. The derived delta expression, $\Delta^{\mathrm{DD,Watanabe}}_{\mathrm{implied}}$, given by (2.8) can be seen to very closely match the exact delta, $\Delta^{\mathrm{DD,exact}}_{\mathrm{implied}}$, which indicates that the expression accurately approximates the delta of an option across a range of strikes.

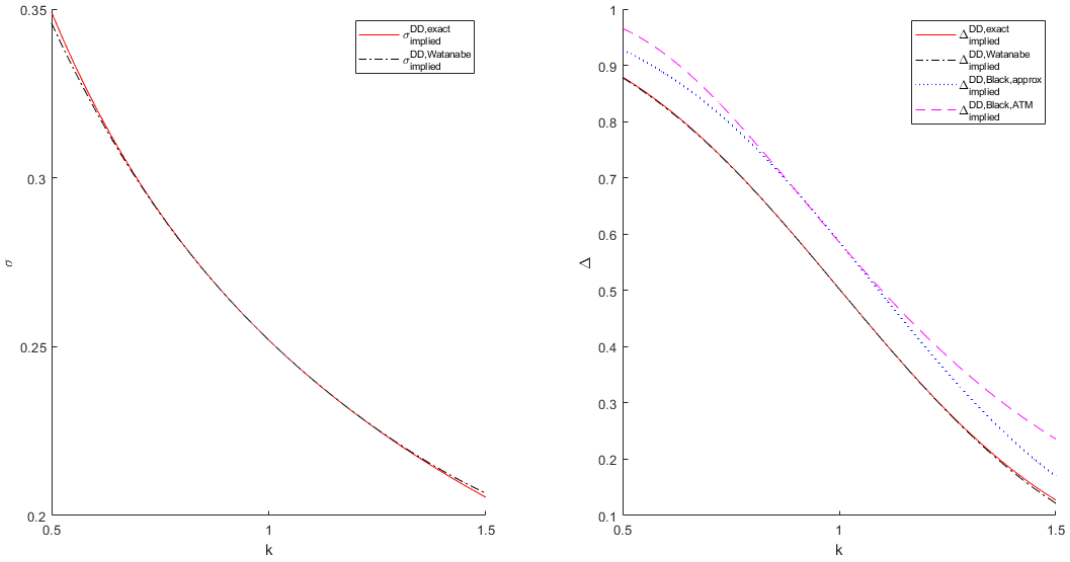

Fig. 3.6: Implied volatilities using Watanabe's expansion, (2.5) (black, dash-dot) compared to exact implied volatility solutions (red, solid) on the left. On the right is the delta computed using (2.8) (black, dash-dot) compared to the exact delta (red, solid), the approximate Black delta (blue, dot) and the at-the-money Black delta (pink, dash). The parameters for these plots are: $\sigma_0 = 1/4$, $\beta = 1/32$, $\alpha = 0$ and $T = 3$.

3.3.5 Volatility Smiles

As mentioned in Chapter 1, volatility modelling is often used to describe a market-observed implied volatility smile. The Hyp-Hyp model can be used in this regard. In Jäckel and Kahl (2008), the primary result is a plot of implied volatility as a function of strike. The implied volatility is plotted as a function of $k := K/S_0$, as opposed to K, in order to normalise the strike as a function of the initial value of the underlying. Because k is defined in this way, high values of k (that is, values significantly larger than 1) represent far out-the-money options while low values of k represent far in-the-money options.

Firstly, a Monte Carlo simulation of the SDEs (2.1) and (2.2) is plotted for a range of strikes. The Monte Carlo is implemented as outlined in Section 3.3.2 and gives the volatility smile that is produced by the model SDEs. In both Sections 3.3.5 and 3.3.6, the antithetic variates variance reduction technique was used in the Monte Carlo simulation. Alongside this plot, the implied volatility from the analytical approximations is plotted for comparison. In this way, the accuracy of the approximation can be assessed by comparing these results to those of the Monte Carlo.

As seen in Section 3.3.3, the hyperbolically scaled analytical approximation, (2.7), most closely matches the Monte Carlo results for at-the-money options. For this reason, this implied volatility approximation is used to approximate the volatility smile. The approximation is referred to as the "Quartic Hyp-Hyp" model in the figures due to the local volatility terms in the Watanabe approximation being quartic in terms of z (and thus in terms of k). The Monte Carlo and approximation plots, as well as the absolute error between the two, are plotted in Figure 3.7. In the volatility smile plots, the axis on the right hand side gives the error between the approximation and the Monte Carlo values for implied volatility while the left hand axis gives the implied volatility.

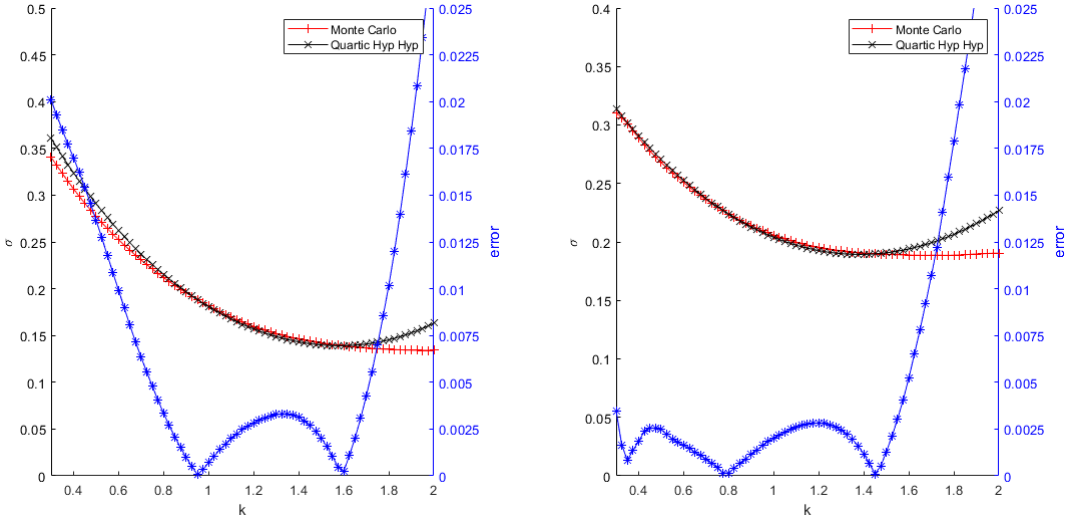

Fig. 3.7: Implied volatilities using the hyperbolically scaled approximation (2.7) (black, crosses) compared to Monte Carlo implied volatilities (red, pluses). The parameters on the left are $\beta = 3/10$, $\alpha = 1/2$, $\kappa = 1$, $\sigma_0 = 4/25$, $\rho = -1/2$ and $T = 3$ while the parameters on the right are $\beta = 7/10$, $\alpha = 3/10$, $\kappa = 1$, $\sigma_0 = 1/5$, $\rho = -3/10$ and $T = 1$. The Monte Carlo used a stepsize of $\Delta t = 1/10$ and $N = 2^{17} - 1$ sample paths with antithetic variates.

Figure 3.7 shows that the analytical approximation, (2.5), scaled with (3.11) is reasonably accurate especially for at-the-money and near-the-money options. This level of accuracy is considered to be well within the accuracy required for practical purposes. As can be seen in the figure, however, the approximation is less accurate especially for far out-the-money options. These trends are true for both smiles produced by the sets of parameters above. The implied volatility for far out-the-money options can be adjusted using an SVI projection as outlined by Gatheral (2004) and

mentioned in Section 2.2. However, far out-the-money options (for which the implied volatilities are plotted) have very little value to begin with and the use of an SVI projection was not considered within the scope of this dissertation.

3.3.6 Time Dependent Parameters

As discussed in Jäckel and Kahl (2008), the calibration of model parameters to market implied volatility surfaces requires the introduction of a time-dependent model parameter. This is done in order to minimise the error between the market-observed implied volatility surfaces and the volatility surface constructed from the model (via the approximations). As market implied volatility surfaces change over time, so too should the implied volatility surface produced by the Hyp-Hyp model. It is thus suggested that the parameter σ_0 is defined as a function dependent on time. In this sense, σ_0 can be interpreted as an instantaneous volatility. The definition of σ_0 as a function as opposed to a constant adds flexibility to the Hyp-Hyp model that, in turn, allows it to more accurately capture market implied volatility surfaces.

According to Jäckel and Kahl (2008), the realised variance, $\|\sigma\|_2$, is used to approximate the constant volatility for a given function $\sigma_0(t)$. The realised variance is computed using

$$\|\sigma\|_2 = \sqrt{\frac{1}{T}\int_0^T \sigma_0(s)ds}. \tag{3.19}$$

When the Watanabe and Fouque approximations are used, the integral in (3.19) can be computed using numerical integration. In the case of the joint Monte Carlo simulation, however, the realised variance need not be used as an approximation for the constant volatility as the function, $\sigma_0(t)$, can simply be evaluated at each time step. The resulting plots, using affine functions to describe $\sigma_0(t)$, are plotted in Figure 3.8.

In addition to introducing time dependence in order to calibrate to market implied volatilities, the $\sigma_0(t)$ functions have shifted the implied volatilities from Figure 3.7 up and down due to $\sigma_0(t)$ being the volatility level parameter. As can be seen in Figure 3.8, the introduction of a time dependent parameter and the vertical shift of implied volatilities does not significantly affect the conclusions drawn in Section 3.3.5.

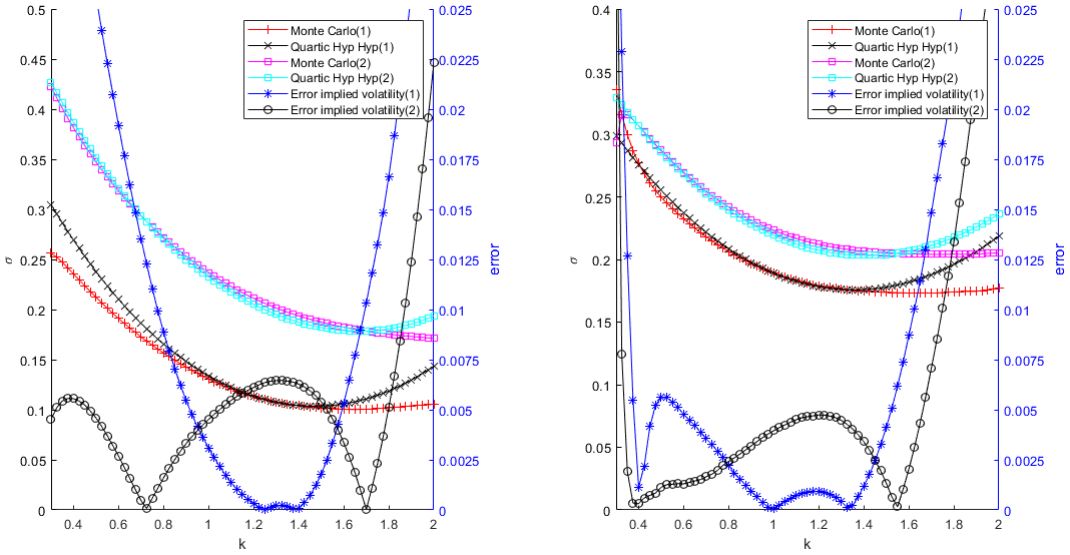

Fig. 3.8: Implied volatilities using the hyperbolically scaled approximation (2.7) (black, crosses and blue, squares) compared to Monte Carlo implied volatilities (red, pluses and pink, squares). The parameters on the left are $\beta = 3/10$, $\alpha = 1/2$, $\kappa = 1$, $\sigma_{0,(2)/(1)}(t) = 4/25 \pm 3/100$, $\rho = -1/2$ and $T = 3$ while the parameters on the right are $\beta = 7/10$, $\alpha = 3/10$, $\kappa = 1$, $\sigma_{0,(2)/(1)}(t) = 1/5 \pm 3/100$, $\rho = -3/10$ and $T = 1$. The Monte Carlo used a stepsize of $\Delta t = 1/10$ and $N = 2^{17} - 1$ sample paths with antithetic variates.

Chapter 4

Extended Analysis and Results

After implementing the Hyp-Hyp model, this dissertation analyses the model in more detail. Chapter 3 presented more detail on how the model is implemented while the present chapter makes use of the implemented model to provide further analysis of the Hyp-Hyp model and the analytical approximation. Section 4.1 firstly considers the derivation of various other sensitivity expressions along the lines of the derivation of an expression for the delta outlined in Section 3.3.4. In this section, a local volatility surface using these expressions is also produced. In Section 4.2, the effect of each of the model parameters on the model output (that is, the volatility smile) is investigated. Lastly, in Section 4.4, the accuracy of the approximation is assessed for functional forms other than those proposed for the Hyp-Hyp model. It is in this final section that hyperbolic-local and hyperbolic-stochastic volatility are assessed independently of one another.

4.1 Sensitivities

As an extension to the original delta expression, (2.8), this dissertation provides similar expressions for other sensitivities, $\frac{\partial v}{\partial T}$, $\frac{\partial v}{\partial K}$ and $\frac{\partial^2 v}{\partial K^2}$.

In a similar manner to the delta expression derivation in Jäckel and Kahl (2008), the partial derivative of $v(S_0, K, T) = S_0\, B(1, k, \hat{\sigma}, T)$ is taken with respect to K,

$$\frac{\partial v}{\partial K} = S_0 \frac{\partial k}{\partial K}\frac{\partial B}{\partial k} + S_0 \frac{\partial B}{\partial \hat{\sigma}}\frac{\partial k}{\partial K}\frac{\partial \hat{\sigma}}{\partial k},$$

where $k = K/S_0$ and $B = B(1, k, \hat{\sigma}, T)$ as before and $\hat{\sigma} = \hat{\sigma}(\sigma_0, k, T, f_1, f_2, f_3, f_4)$. Using the fact that $\frac{\partial k}{\partial K} = 1/S_0$, an expression for the strike sensitivity, $\frac{\partial v}{\partial K}$, of a European option is given by

$$\frac{\partial v}{\partial K} = \frac{\partial B}{\partial k} + \frac{\partial B}{\partial \hat{\sigma}}\frac{\partial \hat{\sigma}}{\partial k}, \tag{4.1}$$

where, as before, $\frac{\partial B}{\partial k}$, $\frac{\partial B}{\partial \hat{\sigma}}$ and $\frac{\partial \hat{\sigma}}{\partial k}$ can be evaluated using central differencing. Taking partial derivatives again, the expression for the second order strike sensitivity, $\frac{\partial^2 v}{\partial K^2}$,

is given by

$$\frac{\partial^2 v}{\partial K^2} = \frac{\partial k}{\partial K}\frac{\partial^2 B}{\partial k^2} + \frac{\partial k}{\partial K}\frac{\partial \hat{\sigma}}{\partial k}\frac{\partial^2 B}{\partial \hat{\sigma}\partial k} + \frac{\partial k}{\partial K}\frac{\partial^2 \hat{\sigma}}{\partial k^2}\frac{\partial B}{\partial \hat{\sigma}} + \frac{\partial \hat{\sigma}}{\partial k}\left[\frac{\partial k}{\partial K}\frac{\partial \hat{\sigma}}{\partial k}\frac{\partial^2 B}{\partial \hat{\sigma}^2} + \frac{\partial k}{\partial K}\frac{\partial^2 B}{\partial \hat{\sigma}\partial k}\right]$$
$$= \left[\frac{\partial^2 B}{\partial k^2} + 2\frac{\partial \hat{\sigma}}{\partial k}\frac{\partial^2 B}{\partial \hat{\sigma}\partial k} + \frac{\partial^2 \hat{\sigma}}{\partial k^2}\frac{\partial B}{\partial \hat{\sigma}} + \left(\frac{\partial \hat{\sigma}}{\partial k}\right)^2\frac{\partial^2 B}{\partial \hat{\sigma}^2}\right] \Big/ S_0. \tag{4.2}$$

Lastly, the expression for theta is

$$\frac{\partial v}{\partial T} = S_0\frac{\partial B}{\partial T} + S_0\frac{\partial \hat{\sigma}}{\partial T}\frac{\partial B}{\partial \hat{\sigma}}. \tag{4.3}$$

As was done with the delta, the sensitivities are plotted as a function of strike. They are plotted for the DD functional forms as this allows them to be compared to the closed form solutions for these sensitivities. As with the delta, central finite differencing is used to evaluate the partial derivatives $\frac{\partial B}{\partial k}$, $\frac{\partial B}{\partial \hat{\sigma}}$, $\frac{\partial \hat{\sigma}}{\partial k}$ and $\frac{\partial \hat{\sigma}}{\partial T}$ as well as the second order partial derivatives $\frac{\partial^2 B}{\partial k^2}$, $\frac{\partial^2 B}{\partial \hat{\sigma}\partial k}$, $\frac{\partial^2 \hat{\sigma}}{\partial k^2}$ and $\frac{\partial^2 B}{\partial \hat{\sigma}^2}$. These plots are shown in Figures 4.1 and 4.2.

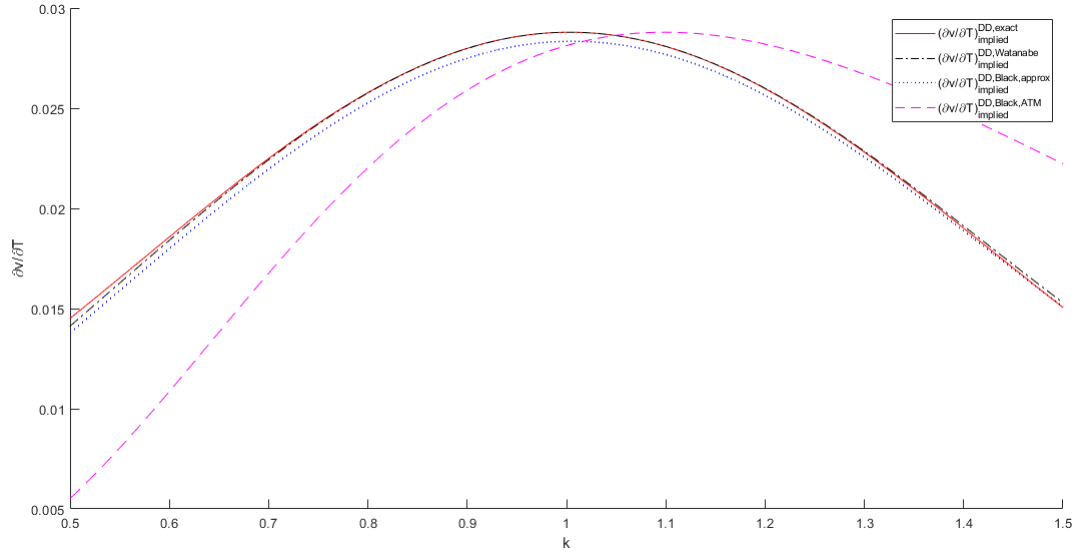

Fig. 4.1: The theta computed using (4.3) (black, dash-dot) compared to the exact theta (red, solid), the approximate Black theta (blue, dot) and the at-the-money Black theta (pink, dash). The parameters for this plot are: $\sigma_0 = 1/4$, $\beta = 1/32$, $\alpha = 0$ and $T = 3$.

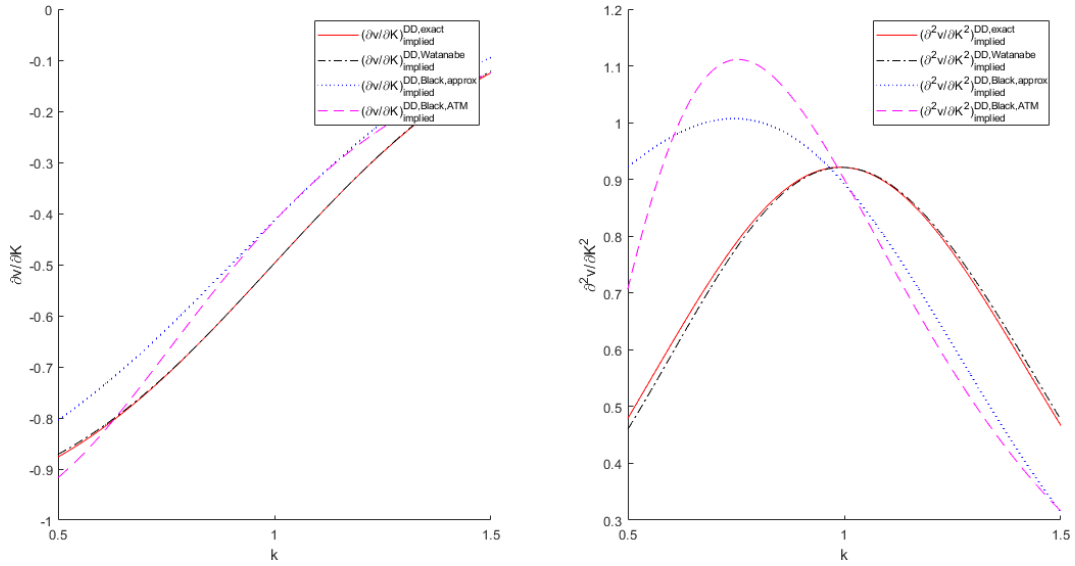

Fig. 4.2: The strike sensitivity computed using (4.1) (black, dash-dot) compared to the exact strike sensitivity (red, solid), the approximate Black strike sensitivity (blue, dot) and the at-the-money Black strike sensitivity (pink, dash) on the left and the second order strike sensitivity computed using (4.2) (black, dash-dot) compared to the exact second order strike sensitivity (red, solid), the approximate second order Black strike sensitivity (blue, dot) and the second order at-the-money Black strike sensitivity (pink, dash) on the right. The parameters for these plots are: $\sigma_0 = 1/4$, $\beta = 1/32$, $\alpha = 0$ and $T = 3$.

As with the delta expression, although Figures 4.1 and 4.2 are given for the DD functional forms, the approximations are applicable to the functional forms describing the Hyp-Hyp model. The accuracy of the approximations is simply confirmed by the DD functional forms. The above sensitivities fully describe the local volatility surface via the Dupire equation, (1.1). The sensitivity expressions ((4.1), (4.2) and (4.3)) are used in conjunction with the Dupire equation to plot a local volatility surface. This local volatility surface is given by Figure 4.3.

The local volatility surface below is a generalisation of the constant volatility assumption of the Black-Scholes model. The surface simply gives the volatility for each maturity and strike that is used in order to model the volatility smile.

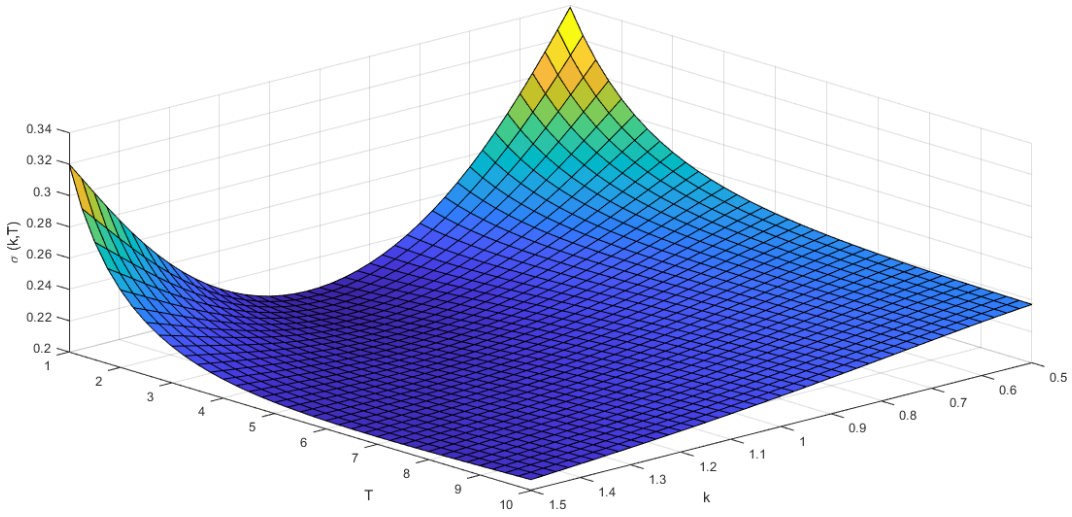

Fig. 4.3: The local volatility surface produces using the Dupire equation, (1.1), and the expressions for sensitivities given by (4.3), (4.1) and (4.2). The parameters for the surface are $\sigma_0 = 1/5$, $\kappa = 1/2$, $\alpha = 3/5$, $\beta = 1$ and $\rho = 0$.

.

4.2 Analysis of Parameters

An analysis of the model parameters, $\Omega_{\text{hyp}-\text{hyp}}$, is presented in the following section. The output of the model is considered to be a volatility smile as shown in Figure 3.7. The Monte Carlo values for implied volatility are not considered in this section as the implied volatility from the approximation was deemed to be accurate enough for practical purposes in Section 3.3.5. The analytical approximation used for the analyses in this section is the scaled version of the Watanabe and Fouque approximations given by (2.7). In this sense, the analytical approximation is useful as a tool to analyse the effects of these model parameters. It is preferred to a Monte Carlo simulation in that it has little to no computational limitations and any error in the approximation is not specific to the sample used (as would be the case in a Monte Carlo simulation). In analysing the effect of each parameter, the base set of parameters used are: $\beta = 3/10$, $\alpha = 1/2$, $\kappa = 1$, $\sigma_0 = 4/25$, $\rho = -1/2$ and $T = 3$. These are the same parameters used in the left hand plot of Figure 3.7 so that the results can use this plot as a reference point. In order to analyse the effect of each parameter in isolation, each parameter is varied while all of the other parameters are kept at their base level.

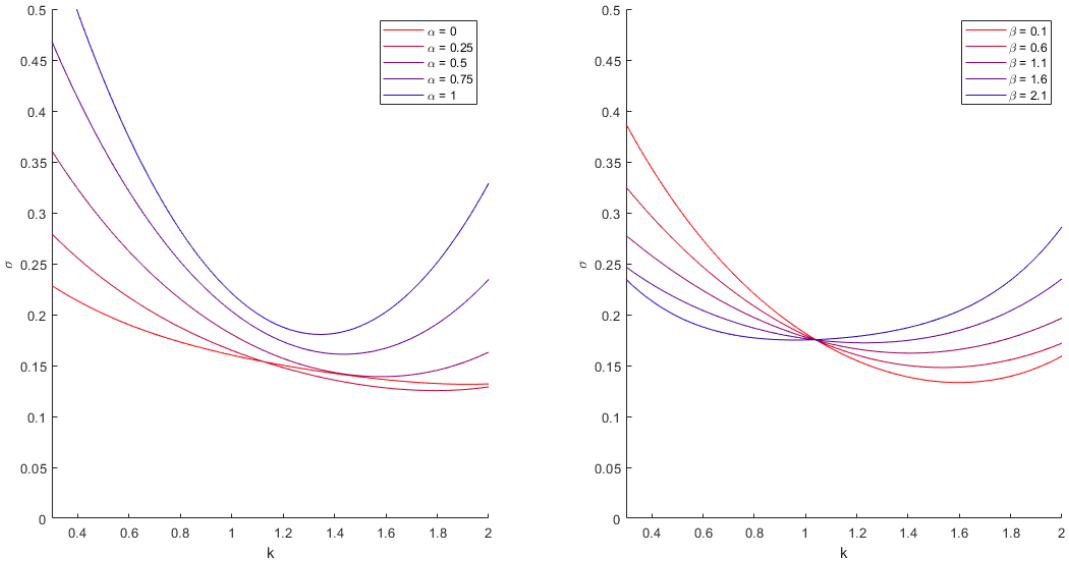

Fig. 4.4: Implied volatilities using the hyperbolically scaled approximation (2.7). The parameters on the left are $\beta = 3/10$, $\kappa = 1$, $\sigma_0 = 4/25$, $\rho = -1/2$ and $T = 3$ with varying α while the parameters on the right are $\alpha = 1/2$, $\kappa = 1$, $\sigma_0 = 4/25$, $\rho = -1/2$ and $T = 3$ with varying β.

Firstly, the effects of α and β on the volatility smile are considered. The volatility smiles produced from varying the levels of these two parameters are shown in Figure 4.4. As can be seen above, increasing α increases the curvature of the volatility smile. When $\alpha = 0$, the implied volatility seems to be an almost flat function of k while when $\alpha = 1$, the volatility smile is highly convex. The model SDEs, (2.1) and (2.2), make used of the parameter α to describe the volatility of the volatility driver, y_t. As alluded to in Section 1.2, stochastic volatility is generally used to capture the curvature of a volatility smile. This can be seen in the left hand plot of Figure 4.4 in that, by increasing the volatility of the stochastic volatility (through an increase in α), the curvature of the volatility smile is increased. In addition to this, an increase in α shifts the volatility level up slightly. This is especially noticeable for at-the-money implied volatilities (that is, when $k = 1$).

Considering the right hand plot of Figure 4.4, an increase in β can be seen to shift the skew of the volatility smile. Specifically, a low β has a smile that is centered around higher values of k while a high β has a smile that is centered around low values of k. The parameter β is only incorporated into the Hyp-Hyp model through the local volatility function, (2.3). As such, β can be described as a local volatility parameter. This is discussed more in Section 4.4.2. Jäckel and Kahl (2008) mention that local volatility is generally used to model the skew of a volatility smile. This can be seen from the fact that β, the only purely local volatility parameter, directly

effects the skew of the volatility smile. A second observation is that, for all values of β, the smile passes through the same point for an at-the-money option. This is because, for an at-the-money option, $k = 1$. For the hyperbolic-local volatility function (2.3), the initial condition was that $f(1) = 1$ for all values of β. Consequently, for an at-the-money option ($k = 1$), the parameter β does not effect the price of the option and therefore has no effect on the implied volatility.

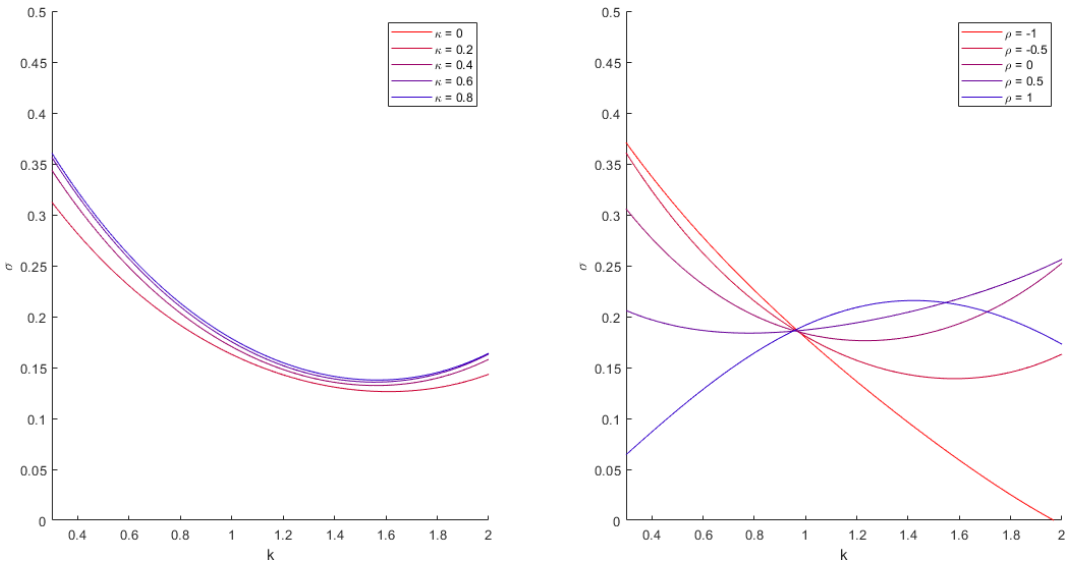

Fig. 4.5: Implied volatilities using the hyperbolically scaled approximation (2.7). The parameters on the left are $\alpha = 1/2$, $\beta = 3/10$, $\sigma_0 = 4/25$, $\rho = -1/2$ and $T = 3$ with varying κ while the parameters on the right are $\alpha = 1/2$, $\beta = 3/10$, $\kappa = 1$, $\sigma_0 = 4/25$ and $T = 3$ with varying ρ.

As can be seen in the left hand plot of Figure 4.5, the effect of changing κ is far less significant than the effect of any of the other model parameters on the implied volatility. As with α, the parameter κ is used to describe the stochastic volatility through the SDE for the volatility driver, (2.2). As with α, an increasing κ seems to increase both the level and the curvature of the volatility smile, although the effect is a lot less drastic than that of α. This effect is due to κ forming part of the diffusion term of (2.2) and thus the volatility of the volatility driver. In addition to this, κ also represents the rate of mean reversion in the SDE (2.2).

At this point, it is useful to discuss the mean reversion of the volatility driver, y_t. Firstly, from the SDE, it can be seen that y_t mean reverts to 0. This is not, however, the level to which the volatility mean reverts (as would be the case in the Heston model, for example). This is due to the hyperbolic-stochastic volatility function (2.4) and the fact that, when $y_t = 0$, the initial value of the function is $g(0) = 1$.

Therefore, as y_t mean reverts to 0, the stochastic volatility function mean reverts to 1 that, in the absence of local volatility, would result in the volatility in SDE (2.1) mean reverting to σ_0. The parameter κ can be interpreted as influencing the rate of mean reversion of the volatility to σ_0 but this mean reversion is also dictated by the functional form of $g(y)$.

The right hand plot of Figure 4.5 shows that the value of ρ affects the convexity of the volatility smile. An imperfect negative correlation (for example, $\rho = -0.5$), results in a convex smile that seems to most accurately capture the shape of market observed volatility smiles. That is, this specific shape is able to accurately capture the higher implied volatilities for far in-the-money and far out-the-money options that occur in the market. A negative value of ρ is therefore in line with the "leverage effect", which proposes that the volatility of an asset increases as the value of the asset decreases (Black, 1976). Simply put, Black (1976) explains that, as the value of a firm declines (analogous to x_t decreasing), it becomes more highly leveraged, thus increasing the volatility of x_t.

In addition to affecting the convexity, the "average slope" of the volatility smile is also affected by ρ. In the Heston (1993) model, a negative correlation decreases the price (and implied volatility) of out-the-money options relative to in-the-money options. This trend is seen by the fact that a perfectly negative correlation, $\rho = -1$, results in an almost flat downward sloping smile. A positive correlation in the Heston model results in higher prices (and implied volatilities) for out-the-money options than in-the-money options. This trend can also be seen for $\rho = 0.5$ and $\rho = 1$ for the Hyp-Hyp model in that these correlations result in upward sloping volatility smiles.

Lastly, the effect of σ_0 on the volatility smile is illustrated in Figure 4.6. This figure shows a very simple effect that the parameter σ_0 has on the volatility smile. An increasing value of σ_0 simply increases the level of the volatility smile. This is because σ_0 is the volatility level parameter. As mentioned in the discussion on the mean reversion of stochastic volatility above, σ_0 is simply the level to which volatility mean reverts.

To summarise this section, the individual model parameters are analysed in isolation. While κ has a very small effect on the volatility smile, the effects of the other parameters are explained. Notably, α is used to capture the curvature of a volatility smile, β is used to capture the skew and ρ describes the shape by effecting the convexity. The level of the volatility smile is described by σ_0.

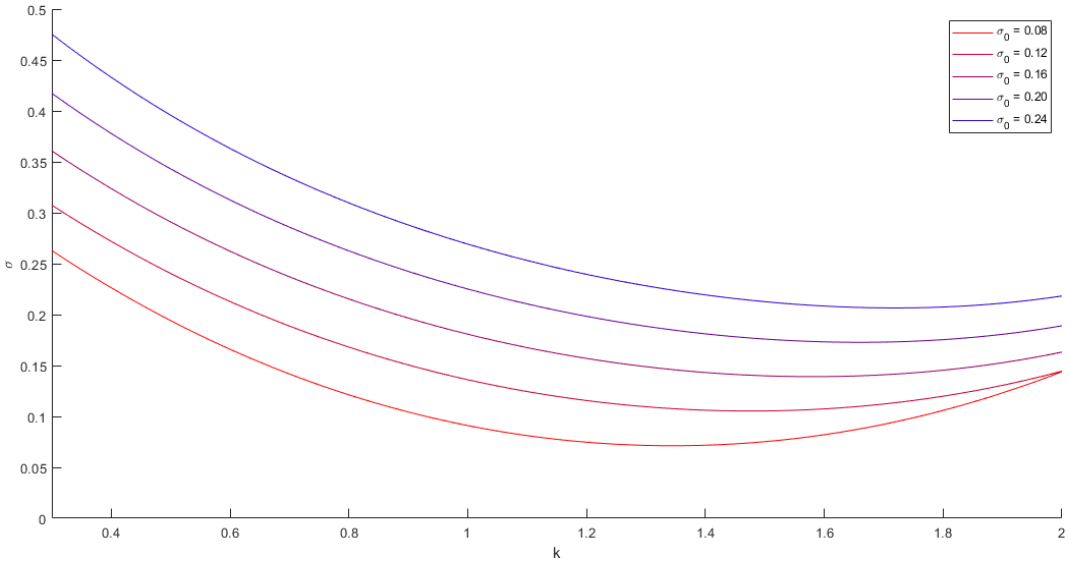

Fig. 4.6: Implied volatilities using the hyperbolically scaled approximation (2.7). The parameters are $\alpha = 1/2$, $\kappa = 1$, $\beta = 3/10$, $\rho = -1/2$ and $T = 3$ with varying σ_0.

4.3 Implied Volatility Surface

Figure 4.7 shows the effect that the maturity of an option has on the volatility smile. As can be seen, an increase in the maturity, T, of an option decreases the curvature of the volatility smile. According to Hull (2003), as maturity increases, the impact of non-constant volatility becomes less pronounced on implied volatilities thus resulting in a flatter volatility smile for longer maturities.

Figure 4.7 can also be plotted as a surface to yield the implied volatility surface for the Hyp-Hyp model, as in Figure 4.8. The implied volatility surface shows the same trends as the previous plot. The figure shows the volatility smile that exists across a range of maturities. Specifically, far out-the-money and far in-the-money options have higher implied volatilities, especially for shorter maturities. In a Black-Scholes world, this surface would be flat.

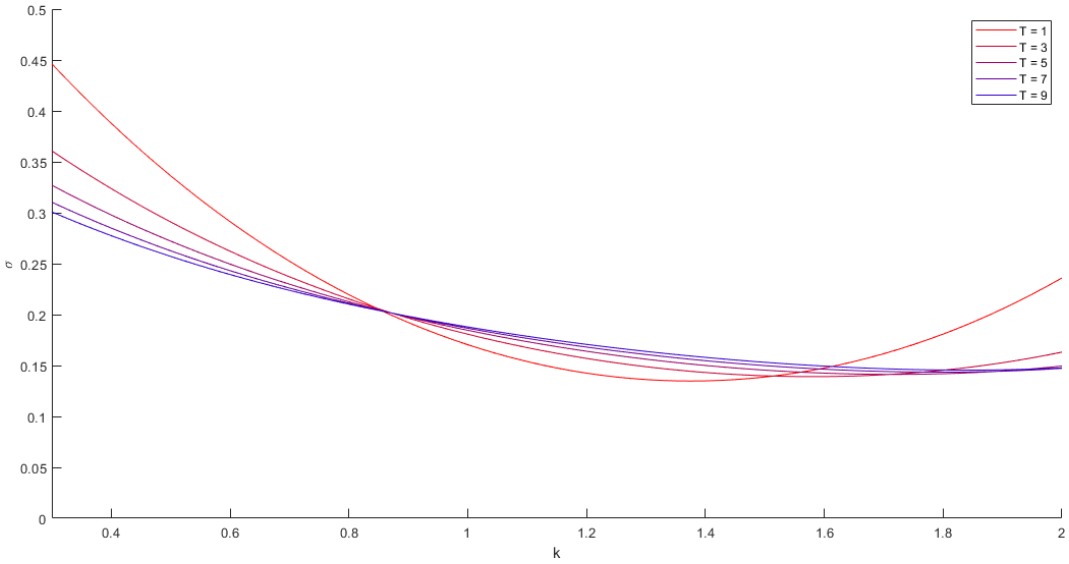

Fig. 4.7: Implied volatilities using the hyperbolically scaled approximation (2.7). The parameters are $\alpha = 1/2$, $\kappa = 1$, $\beta = 3/10$, $\sigma_0 = 4/25$ and $\rho = -1/2$ with varying T.

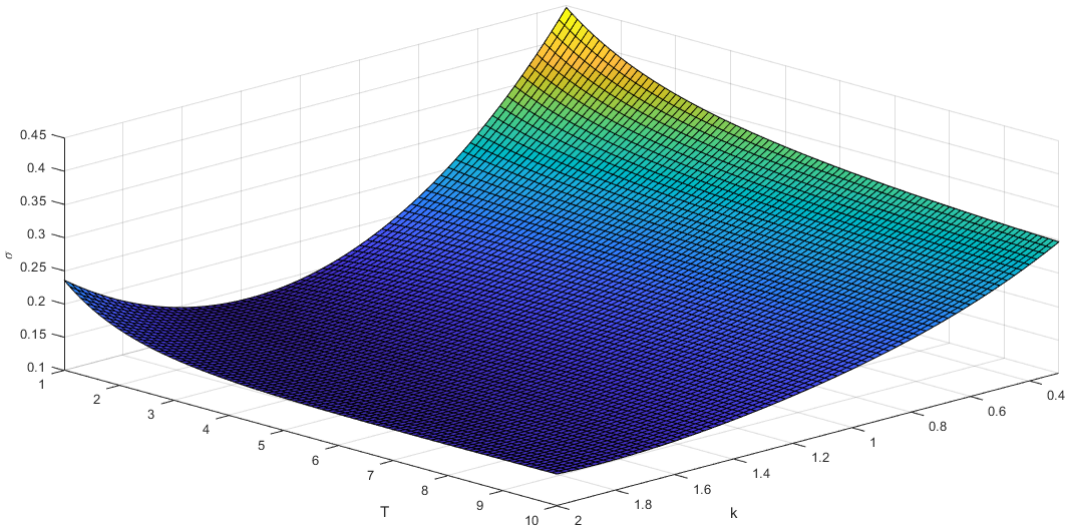

Fig. 4.8: Implied volatility surface using the hyperbolically scaled approximation (2.7). The parameters are $\alpha = 1/2$, $\kappa = 1$, $\beta = 3/10$, $\sigma_0 = 4/25$ and $\rho = -1/2$.

4.4 Analysis of Approximation for Different Functional Forms

In this section, the accuracy of the analytical approximation scaled using (2.7) is investigated for alternative functional forms (as opposed to the Hyp-Hyp model functional forms). Importantly, for this section, the functional forms considered need to agree with the functional forms of the Hyp-Hyp model at the initial conditions. That is, it is required that $f(1) = 1$ and that $g(0) = 1$. This is because the approximation is derived assuming that these are the initial values of the two functions. In addition to this, the SDE described by (2.1),

$$dx_t = \sigma_0 f(x_t) g(y_t) dW_t,$$

has an initial volatility of σ_0 if these initial values of the functional forms are met.

4.4.1 CEV and SABR Functional Forms

First, the functional forms describing the SABR and CEV model are considered. The functional forms used are $f(x) = x^\beta$ for the CEV model and $g(y) = e^y$ for the SABR model. These two functional forms are considered in conjunction with one another because separation of purely local and purely stochastic volatility functional forms is considered in the next section. The volatility smile for the CEV and SABR functional forms is plotted in Figure 4.9 using both the analytical approximation and a Monte Carlo simulation.

Figure 4.9 shows that the analytical approximation is able to produce a volatility smile that is reasonably close to that produced by the Monte Carlo simulation. Despite the approximation for implied volatility being reasonably close to the Monte Carlo plot, the approximation is not as accurate for the CEV and SABR functional forms as it is for the Hyp-Hyp functional forms. This can be seen by comparing Figure 4.9 to the left hand plot of Figure 3.7.

The volatility smile produced by the approximation is almost identical to that produced by the approximation for the Hyp-Hyp functional forms. This is because the derivatives of the CEV and SABR functional forms that are used in the approximation, that is $f_i = f^{(i)}(1)$ and $g_i = g^{(i)}(0)$, are largely similar to those of the Hyp-Hyp functional forms. For the CEV functional form, the first two derivatives can be shown to be: $f_1 = \beta$ and $f_2 = \beta(\beta - 1)$, which are identical to the first two derivatives of the hyperbolic-local functional form given at the beginning of Section 3.3.1. Although the higher order derivatives are not identical to the hyperbolic-local volatility higher order derivatives, the approximation is still almost identical

because the higher order derivatives have less significant contributions to the implied volatility: in Watanabe's expansion, (2.5), the higher order derivatives only form a part of the $\hat{\sigma}_{3,\mathrm{sl}}$ and $\hat{\sigma}_{4,\mathrm{sl}}$ local volatility terms. The SABR functional form agrees with the hyperbolic-stochastic volatility form exactly in that $g_1 = g_2 = 1$.

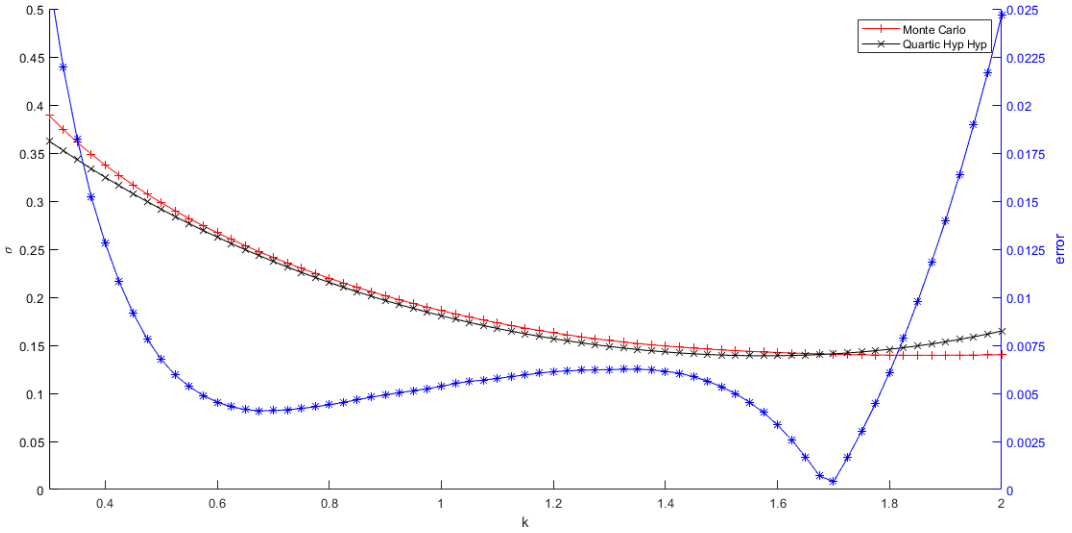

Fig. 4.9: Implied volatilities using the hyperbolically scaled approximation (2.7) (black, crosses) compared to the Monte Carlo implied volatility (red, pluses) for the CEV and SABR functional forms . The parameters are $\alpha = 1/2$, $\kappa = 1$, $\beta = 3/10$, $\sigma_0 = 4/25$, $\rho = -1/2$ and $T = 3$. The Monte Carlo used a stepsize of $\Delta t = 1/10$ and $N = 2^{16} - 1$ sample paths with antithetic variates.

4.4.2 Local and Stochastic Volatility in Isolation

In this section, the hyperbolic-local volatility and hyperbolic-stochastic volatility are considered in isolation of one another. Firstly, in order to consider only local volatility, the hyperbolic-stochastic volatility function is set to $g(y) = 1$, resulting in a purely hyperbolic-local volatility model defined by the SDE

$$dx_t = \sigma_0 f(x_t) dW_t, \tag{4.4}$$

where $f(x)$ is defined as in (2.3).

Secondly, when considering hyperbolic-stochastic volatility, the local volatility function is set to $f(x) = x$ such that the hyperbolic-stochastic volatility model SDE is given by

$$dx_t = \sigma_0 g(y_t) x_t dW_t, \tag{4.5}$$

with y_t following the dynamics described by (2.2) and $g(y)$ defined by (2.4), as before. The reason that $f(x)$ takes on this functional form is that the diffusion term in a forward Black-Scholes SDE is dependent on the value of the underlying, x_t. The above SDE describes the forward Black-Scholes dynamics with hyperbolic-stochastic volatility, $\sigma_0 g(y_t)$. In fact, to define $f(x) = x$, the same hyperbolic-local volatility function, (2.3), can be used with $\beta = 1$. The plots in Figure 3.5 in Section 3.3.3 therefore only consider hyperbolic-stochastic volatility as they make use of a β parameter of 1. The SDEs (4.4) and (4.5) result in the volatility smiles in Figure 4.10.

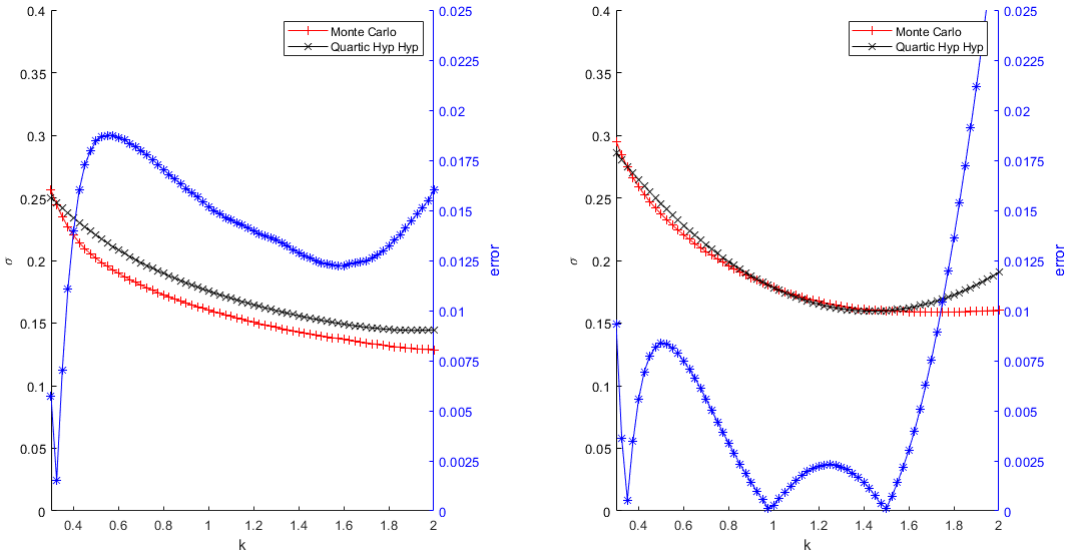

Fig. 4.10: Implied volatilities using the hyperbolically scaled approximation (2.7) (black, crosses) compared to the Monte Carlo implied volatility (red, pluses) for the hyperbolic-local (left) and hyperbolic-stochastic (right) functional forms. The parameters are $\alpha = 1/2$, $\kappa = 1$, $\beta = 3/10$, $\sigma_0 = 4/25$, $\rho = -1/2$ and $T = 3$. The Monte Carlo used a stepsize of $\Delta t = 1/10$ and $N = 2^{16} - 1$ sample paths with antithetic variates.

The effects of hyperbolic-local and hyperbolic-stochastic volatility on the shape of a volatility smile can be seen by considering them in isolation of one another as in Figure 4.10. It is worth noting that the local volatility smile (on the left) is a downward sloping smile with very little curvature. This reaffirms the assertion made by Jäckel and Kahl (2008) that local volatility is used to capture the skew of a volatility smile as opposed to the curvature. This result further enforces the discussion on the local volatility parameter, β, in Section 4.2. The hyperbolic-stochastic volatility smile (on the right) seems to look more similar to the combined hyperbolic-local hyperbolic-stochastic volatility smile in Figure 3.7. This indicates

that hyperbolic-stochastic volatility potentially has a more significant impact on the combined hyperbolic-stochastic hyperbolic-local volatility smile than hyperbolic-local volatility does. The initial skew (that is, the fact that the smile is not centred at $k = 1$) of the hyperbolic-stochastic volatility smile is due to the asymmetrical nature of the hyperbolic-stochastic function, (2.4).

The analytical approximation clearly does not compute the isolated hyperbolic-local volatility functional form particularly accurately when compared to the Monte Carlo simulation. In contrast to this, the analytical approximation seems to compute the hyperbolic-stochastic volatility reasonably well. For hyperbolic-stochastic volatility, once again, the approximation is particularly accurate for at-the-money and near-the-money options while it is less accurate for far out-the-money options. As with the hyperbolic-local hyperbolic-stochastic volatility smile given in Figure 3.7, the inaccuracy for far out-the-money options could be corrected for using an SVI projection should the need arise. Jäckel and Kahl (2008) explain that the analytical approximation is particularly accurate for computing implied volatilities for the hyperbolic-stochastic volatility function, (2.4). This is because this function has higher order derivatives (from the third derivative and higher) that equal 0. The hyperbolic-local volatility function, (2.3), in contrast, has higher order derivatives that influence the implied volatility but are not captured by the analytical approximation, which only contains up to fourth order derivatives of $f(x)$ despite two extra terms for local volatility, $\hat{\sigma}_{3,\text{sl}}$ and $\hat{\sigma}_{4,\text{sl}}$, being incorporated into the expression. Appendix A.2.3 provides the additional terms in order to better incorporate local volatility into the approximation. Despite this, the loss of accuracy due to the existence of higher order derivatives of $f(x)$, which are not incorporated into the approximation, is why the analytical approximation does not compute implied volatilities for hyperbolic-local volatility as well as for hyperbolic-stochastic volatility.

4.4.3 Other Functional Forms

Finally, the approximation accuracy for functions that do not have well known solutions is investigated. The functional forms considered need to have initial values that agree with the functional forms of the Hyp-Hyp model. That is, it is necessary that $f(1) = 1$ and $g(0) = 1$. For this reason, the functional forms considered are

$$f(x_t) = \frac{(x_t + d)^\beta}{(1 + d)^\beta}, \tag{4.6}$$

which represents a shifted CEV model, and

$$g(y_t) = (y_t + 1)^\gamma, \tag{4.7}$$

which both agree with the initial conditions of the Hyp-Hyp model. As with the previous sections, the volatility smile produced by the analytical approximation is compared to that produced by a Monte Carlo simulation of the SDE specified with these functional forms. The resulting volatility smile is shown in Figure 4.11.

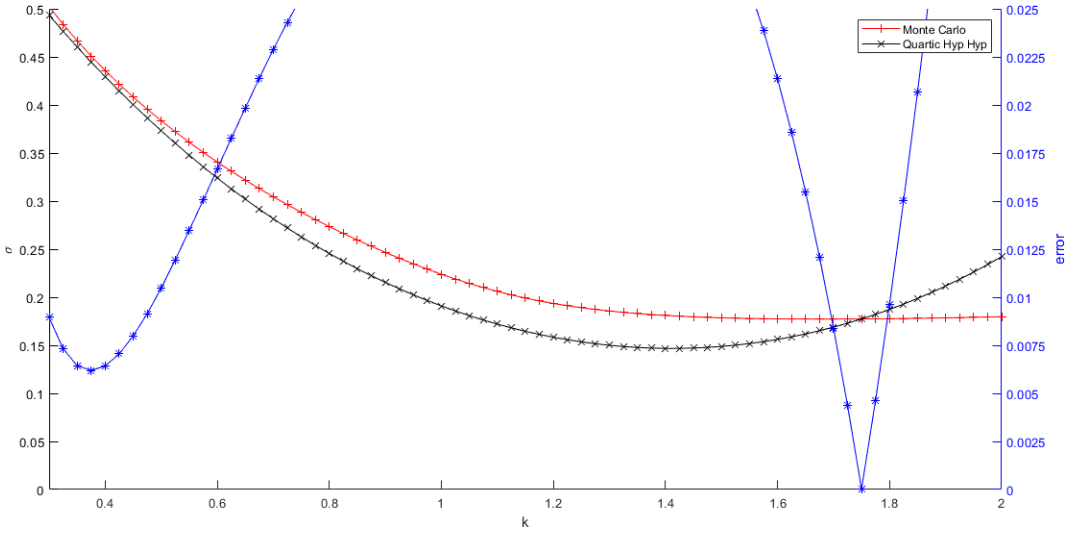

Fig. 4.11: Implied volatilities using the hyperbolically scaled approximation (2.7) (black, crosses) compared to the Monte Carlo implied volatility (red, pluses) for the functional forms, (4.6) and (4.7). The parameters are $\alpha = 1/2$, $\kappa = 1$, $\beta = 3/10$, $\sigma_0 = 4/25$, $\rho = -1/2$, $T = 3$, $d = 1/2$ and $\gamma = 2$. The Monte Carlo used a stepsize of $\Delta t = 1/10$ and $N = 2^{16} - 1$ sample paths with antithetic variates.

The approximation is less accurate for functions (4.6) and (4.7) than it is for the Hyp-Hyp model and for the CEV and SABR functional forms. As discussed, the approximation works particularly well for the Hyp-Hyp model because the stochastic volatility function has vanishing higher order derivatives. In addition, it was proposed in Section 4.4.1 that because the CEV functional form has an f_1 and f_2 that are identical to the Hyp-Hyp model, the approximation works particularly well for this functional form. In contrast, (4.6) and (4.7) have higher order derivatives

$$f_1 = \frac{\beta}{1+d}, \qquad f_2 = \frac{\beta(\beta-1)}{(1+d)^2}, \qquad f_3 = \frac{\beta(\beta-1)(\beta-2)}{(1+d)^3},$$
$$f_4 = \frac{\beta(\beta-1)(\beta-2)(\beta-3)}{(1+d)^4}, \qquad g_1 = \gamma, \qquad g_2 = \gamma(\gamma-1),$$

which do not agree with the Hyp-Hyp functional forms for higher order derivatives. The functions also do not have vanishing higher order derivatives. These reasons are why the approximation is not accurate for (4.6) and (4.7).

Chapter 5

Conclusion

This dissertation explores the details of the Hyp-Hyp model presented by Jäckel and Kahl (2008) as well as an analytical approximation for implied volatility. The advantageous features of the Hyp-Hyp model when compared to the CEV and SABR models are verified. Hyperbolic scaling of the Watanabe and Fouque approximations (based on maturity) for implied volatility is shown to be accurate by comparing it to implied volatility from a Monte Carlo simulation of the Hyp-Hyp model SDEs as a function of both maturity and strike. The expression for the delta of an option based on the Watanabe approximation is shown to be accurate by comparing it to the closed form solution for the DD model. A time dependent model parameter, σ_0, is introduced and used to plot sufficiently accurate volatility smiles.

In line with the work done by Jäckel and Kahl (2008), expressions for the sensitivities $\frac{\partial v}{\partial T}$, $\frac{\partial v}{\partial K}$ and $\frac{\partial^2 v}{\partial K^2}$ are derived and compared to closed form solutions for these sensitivities based on the DD model. Using these expressions, the Dupire equation is used to describe a local volatility surface. The effect of changing each of the model parameters, while keeping all other parameters constant, is investigated using the scaled analytical approximation. In a similar manner, the effect of changing the maturity on the volatility smile is investigated and an implied volatility surface is plotted. Effects of the model parameters and maturity on the volatility smile are in line with what would be expected from literature. The scaled analytical approximation is found to be suitably accurate for a combined CEV and SABR local stochastic volatility model despite it not being as accurate as it is for the Hyp-Hyp model. The analytical approximation captures the shape of a purely local volatility model although it is not particularly accurate. It is, however, sufficiently accurate for a purely stochastic volatility functional form. Lastly, the approximation is shown to be less accurate for other local and stochastic volatility functional forms which do not have higher order derivatives agreeing with the Hyp-Hyp model functional forms.

Bibliography

Black, F. (1976). Studies of stock market volatility changes, *Proceedings of the American Statistical Association Business and Economic Statistics Section* pp. 177–181.

Dupire, B. (1994). Pricing with a smile, *Risk* **7**(1): 18–20.

Finch, S. (2004). Ornstein-Uhlenbeck process, *Unpublished note* pp. 1–2. *Available at* https://oeis.org/A249417/a249417.pdf.

Fouque, J.-P., Papanicolaou, G. and Sircar, K. (2000). *Derivatives in Financial Markets with Stochastic Volatility*, Cambridge University Press.

Gatheral, J. (2004). A parsimonious arbitrage-free implied volatility parameterisation with application to the valuation of volatility derivatives, *TDTF Derivatives Day Amsterdam* .

Hagan, P. S., Kumar, D., Lesniewski, A. S. and Woodward, D. E. (2002). Managing smile risk, *Wilmott* **1**: 84–108.

Heston, S. L. (1993). A closed-form solution for options with stochastic volatility with applications to bond and currency options, *The Review of Financial Studies* **6**(2): 327–343.

Hull, J. C. (2003). *Options futures and other derivatives*, Vol. 8, Prentice Hall.

Jäckel, P. and Kahl, C. (2008). Hyp hyp hooray, *Wilmott Magazine* **34**: 70–81.

Kahl, C. (2007). *Modelling and simulation of stochastic volatility in finance*, PhD thesis, Bergische Universität Wuppertal and ABN AMRO.

Kawai, A. (2002). Analytical and Monte Carlo swaption pricing under the forward swap measure, *Journal of Computational Finance* **6**(1): 101–111.

Osajima, Y. (2006). The asymptotic expansion formula of implied volatility for dynamic SABR model and FX hybrid model, *Technical Report* . University of Tokyo, Graduate School of Mathematical Sciences, Komaba, Tokyo, Japan.

Rubinstein, M. (1983). Displaced diffusion option pricing, *Journal of Finance* **38**(1): 213–217.

Vanyolos, A., Cho, M. and Glasgow, S. A. (2014). Probability density of the CIR model, *Available at SSRN:* http://dx.doi.org/10.2139/ssrn.2508699.

Watanabe, S. (1987). Analysis of Wiener functionals (Malliavin calculus) and its application to heat kernels, *The Annals of Probability* **15**(1): 1–39.

Appendix A

Fouque and Watanabe Approximation Derivations

This appendix gives a detailed derivation of the Fouque, (3.11), and Watanabe, (2.5), approximations. The derivations follow those presented by Kahl (2007) very closely but, in some cases, provide more detail. Section A.1 presents two corrections which directly influence the resulting Fouque approximation given in the body of this dissertation, (3.11). The corrections are typed in red throughout this appendix. The derivation of Watanabe's approximation directly recovers the expression used in the body of this dissertation, (2.5). Kahl (2007) presents the derivation of the Watanabe approximation for a purely stochastic and then purely local volatility model. In order to avoid unnecessary repetition of the derivation presented for these cases, the derivation of the approximation for a local and stochastic volatility model is presented in this dissertation. Kahl (2007) simply provides a result for this case as the derivation follows that of the purely local and purely stochastic volatility model approximations.

A.1 Fouque Approximation

In Section 4.2.7 of Kahl (2007), the Fouque approximation for implied volatility is defined as:

$$\hat{\sigma}_{\text{Fouque}} = ak + b + \mathcal{O}(1/\kappa), \tag{A.1}$$

where $k = \frac{\ln\left(\frac{K}{F}\right)}{T}$. In the same section, a and b are defined as:

$$a = -\frac{V_2}{2\hat{\sigma}_{RMS}^3}, \tag{A.2}$$

and

$$b = \hat{\sigma}_{RMS} - \frac{V_2}{4\hat{\sigma}_{RMS}}, \tag{A.3}$$

respectively. In the same section, (Kahl, 2007) goes on to show that

$$\hat{\sigma}_{RMS}^2 = \sigma_0^2\Big(1 + 2\alpha^2 + \frac{\alpha}{\kappa T}(e^{-2\kappa T} - 1)\Big), \tag{A.4}$$

and

$$V_2 \approx \sigma_0^3(2\alpha^2 + 6\alpha^4 - 2\alpha^6 + 8\alpha^8)\frac{-2\rho}{\alpha\sqrt{2\kappa}}.$$

Rewriting V_2 for the purposes of simplifications which will follow results in

$$\begin{aligned} V_2 &\approx \sigma_0^3 2\alpha^2(1 + 3\alpha^2 - \alpha^4 + 4\alpha^6)\frac{-2\rho}{\alpha\sqrt{2\kappa}} \\ &= 4\sigma_0^3\alpha^2(-4\alpha^6 + \alpha^4 - 3\alpha^2 - 1)\frac{\rho}{\alpha\sqrt{2\kappa}}. \end{aligned} \tag{A.5}$$

Substituting (A.4) and (A.5) into (A.3) and simplifying results in an expression for b:

$$\begin{aligned} b &= \sigma_0\sqrt{1 + 2\alpha^2 + \frac{\alpha^2}{\kappa T}(e^{-2\kappa T} - 1)} - \frac{4\sigma_0^3\alpha^2(-4\alpha^6 + \alpha^4 - 3\alpha^2 - 1)\rho}{4\sigma_0\sqrt{1 + 2\alpha^2 + \frac{\alpha^2}{\kappa T}(e^{-2\kappa T} - 1)}\alpha\sqrt{2\kappa}} \\ &= \sigma_0\sqrt{\frac{(-1 + e^{-2\kappa T})\alpha^2}{T\kappa} + 2\alpha^2 + 1} - \frac{\alpha(-4\alpha^6 + \alpha^4 - 3\alpha^2 - 1)\rho\sigma_0^2}{\sqrt{2\left(\frac{(-1+e^{-2\kappa T})\alpha^2}{T\kappa} + 2\alpha^2 + 1\right)\kappa}}. \end{aligned} \tag{A.6}$$

Similarly, substituting (A.4) and (A.5) into (A.2) and multiplying (A.2) by k results in

$$\begin{aligned} ak &= -\frac{4\sigma_0^3\alpha^2(-4\alpha^6 + \alpha^4 - 3\alpha^2 - 1)\rho}{2\left(\sigma_0^2\left(1 + 2\alpha^2 + \frac{\alpha^2}{\kappa T}(e^{-2\kappa T} - 1)\right)\right)^{3/2}\alpha\sqrt{2\kappa}}\frac{\ln\left(\frac{K}{F}\right)}{T} \\ &= -\frac{\sqrt{2}\sigma_0^3\alpha^2(-4\alpha^6 + \alpha^4 - 3\alpha^2 - 1)\rho}{\sigma_0^3\left(1 + 2\alpha^2 + \frac{\alpha^2}{\kappa T}(e^{-2\kappa T} - 1)\right)^{3/2}\alpha\kappa^{1/2}T}\ln\left(\frac{K}{F}\right) \\ &= -\frac{\sqrt{2}\alpha(-4\alpha^6 + \alpha^4 - 3\alpha^2 - 1)\rho}{\left(\frac{\kappa T + 2\kappa T\alpha^2 + \alpha^2(e^{-2\kappa T} - 1)}{\kappa T}\right)^{3/2}\kappa^{1/2}T}\ln\left(\frac{K}{F}\right) \\ &= -\frac{\sqrt{2}\alpha(-4\alpha^6 + \alpha^4 - 3\alpha^2 - 1)\rho}{\kappa^{-3/2}T^{-3/2}\left(\kappa T + 2\kappa T\alpha^2 + \alpha^2 e^{-2\kappa T} - \alpha^2\right)^{3/2}\kappa^{1/2}T}\ln\left(\frac{K}{F}\right) \\ &= -\frac{\sqrt{2}\alpha(-4\alpha^6 + \alpha^4 - 3\alpha^2 - 1)\rho}{\kappa^{-1}T^{-1/2}\left((2T\kappa + e^{-2T\kappa} - 1)\alpha^2 + T\kappa\right)^{3/2}}\ln\left(\frac{K}{F}\right) \\ &= -\frac{\sqrt{2T}\alpha(-4\alpha^6 + \alpha^4 - 3\alpha^2 - 1)\kappa\rho}{\left((2T\kappa + e^{-2T\kappa} - 1)\alpha^2 + T\kappa\right)^{3/2}}\ln\left(\frac{K}{F}\right). \end{aligned} \tag{A.7}$$

Rewriting (A.1) by substituting in the above expressions for ak and b results in

the final Fouque approximation

$$\hat{\sigma}_{\text{Fouque}} = \sigma_0 \sqrt{\frac{(-1+e^{-2\kappa T})\alpha^2}{T\kappa} + 2\alpha^2 + 1} - \frac{\alpha(-4\alpha^6+\alpha^4-3\alpha^2-1)\rho\sigma_0^2}{\sqrt{2\Big(\frac{(-1+e^{-2\kappa T})\alpha^2}{T\kappa}+2\alpha^2+1\Big)\kappa}} - \frac{\sqrt{2T}\alpha(-4\alpha^6+\alpha^4-3\alpha^2-1)\kappa\rho}{\Big((2T\kappa+e^{-2T\kappa}-1)\alpha^2+T\kappa\Big)^{3/2}} \ln\Big(\frac{K}{F}\Big). \tag{A.8}$$

A.2 Watanabe Approximation

In Section 4.2.5 of Kahl (2007), a derivation for the Watanabe approximation for implied volatility of a local and stochastic volatility model is presented. An asymptotic expansion for x_t based on the model SDEs, (2.1) and (2.2), is given by:

$$x_t = x_0 + \epsilon f_0 \sqrt{t}\big(\tilde{g}_1(t) + \epsilon \tilde{g}_2(t) + \epsilon^2 \tilde{g}_3(t)...\big),$$

where the $\tilde{g}_i(t)'s$ are defined as:

$$\begin{aligned}
\tilde{g}_1(t) &:= \frac{W_t}{\sqrt{t}} \sim \mathcal{N}(0,1),\\
\tilde{g}_2(t) &:= \frac{1}{\sqrt{t}}\left(g_1 \int_0^t y_s dW_s + \sigma_0 f_1 \int_0^t \int_0^s dW_u dW_s\right),\\
\tilde{g}_3(t) &:= \frac{1}{\sqrt{t}}\left(\frac{g_2}{2}\int_0^t y_s^2 dW_s + \sigma_0 g_1 f_1\left(\int_0^t y_s \int_0^s dW_u dW_s + \int_0^t \int_0^s y_u dW_u dW_s\right)\right.\\
&\qquad \left. + \sigma_0^2 f_1^2 \int_0^t \int_0^s \int_0^u dW_v dW_u dW_s + \sigma_0^2 \frac{f_2}{2} f_0 \int_0^t W_s^2 dW_s\right).
\end{aligned}$$

For simplicity, define $f_i := f^{(i)}(x_0)$. The integrals defined above are for a local and stochastic volatility model with the local volatility given by the functional form $f(x)$ and the stochastic volatility given by the functional form $g(y)$. The functions will be defined by the model being considered and the derivation which follows therefore generalises to any local or stochastic volatility model.

In order to determine an approximation for the implied volatility, one can use Watanabe's formula,

$$C_{\text{vol}}(T,K) \approx \epsilon f_0 \sigma_0 \sqrt{T}\, \mathbb{E}\Big[H_0 + \epsilon H_1 \tilde{g}_2 + \epsilon^2\Big(H_1\tilde{g}_3 + \frac{1}{2}H_2\tilde{g}_2^2\Big)\Big], \tag{A.9}$$

where $H_j := H^{(j)}(\tilde{g}_1 - z)$ and $H(x) := x^+$ with

$$z := \frac{K - x_0}{x_0 \sigma_0 \sqrt{T}}.$$

Therefore, one obtains: $H_0 = (\tilde{g}_1 - z)^+$, $H_1 = \mathbb{I}_{\{\tilde{g}_1 \geq z\}}$ and $H_2 = \delta(\tilde{g}_1 - z)$. The formula is based on a similar type expansion done on the SABR model which was

presented by Osajima (2006). It is based on an asymptotic expansion of the value of the underlying asset in terms of some small parameter $\epsilon \ll 1$. Watanabe's method then allows for the price of a European call option to be written as a sum of terms with different powers of ϵ as is presented by (A.9).

An expression for the Black-Scholes implied volatility can be derived by considering Watanabe's formula for the price of a European call option under the Black-Scholes model. The asymptotic Black-Scholes expansion, based on (A.9), can be simplified based on the SDE describing the Black-Scholes model,

$$dx_t = \sigma x_t dW_t, \tag{A.10}$$

where σ is constant. Making use of (A.9), an expression for the price of a European call option based on the Black-Scholes model is given by Kahl (2007):

$$C_{\mathrm{BS}}(T,K) = \epsilon f_0 \hat{\sigma}_0 \sqrt{T}\Big(G(z) + \varphi(z)\big(\epsilon G_1(z,\hat{\sigma}_0,\hat{\sigma}_1) + \epsilon^2 G_2(z,\hat{\sigma}_0,\hat{\sigma}_1,\hat{\sigma}_2)\big)\Big),$$

where $\varphi(x)$ is the standard normal density function and, as given by Kahl (2007), the $G_i(z)$ terms are defined as:

$$G_1(z,\hat{\sigma}_0,\hat{\sigma}_1) = \frac{1}{2}\sqrt{T} z \hat{\sigma}_0 + \frac{\hat{\sigma}_1}{\hat{\sigma}_0}, \tag{A.11}$$

$$\begin{aligned} G_2(z,\hat{\sigma}_0,\hat{\sigma}_1,\hat{\sigma}_2) = {} & \frac{1}{8} T \hat{\sigma}_0^2 z^4 + \frac{1}{2}\sqrt{T}\hat{\sigma}_1 z^3 - \frac{(T\hat{\sigma}_0^4 - 6\hat{\sigma}_1^2) z^2}{12\hat{\sigma}_0^2} \\ & + \frac{1}{2}\sqrt{T}\hat{\sigma}_1 z - \frac{T\hat{\sigma}_0^2}{24} + \frac{\hat{\sigma}_2}{\hat{\sigma}_0}. \end{aligned} \tag{A.12}$$

Matching the terms of (A.9) for a local and stochastic volatility model with the asymptotic Black-Scholes expansion, based on powers of ϵ, one obtains:

$$\begin{aligned} &\hat{\sigma}_0 = \sigma_0, \\ &G(z) = \mathbb{E}[H_0], \\ &\varphi(z) G_1(z,\hat{\sigma}_0,\hat{\sigma}_1) = \mathbb{E}[H_1 \tilde{g}_2], \qquad (A.13) \\ &\varphi(z) G_2(z,\hat{\sigma}_0,\hat{\sigma}_1,\hat{\sigma}_2) = \mathbb{E}\Big[H_1\tilde{g}_3 + \frac{1}{2} H_2 \tilde{g}_2^2\Big]. \qquad (A.14) \end{aligned}$$

In order to determine an expression for $\hat{\sigma}_1$, one expands (A.13) and uses the tower property as well as the expression for $\mathbb{E}[\tilde{g}_2|\tilde{g}_1]$ given in Section 4.2.2.1 of Kahl (2007):

$$\begin{aligned} \varphi(z) G_1(z,\hat{\sigma}_0,\hat{\sigma}_1) &= \mathbb{E}[\mathbb{I}_{\{\tilde{g}_1 \geq z\}} \tilde{g}_2] \\ &= \mathbb{E}\Big[\mathbb{E}[\mathbb{I}_{\{\tilde{g}_1 \geq z\}} \tilde{g}_2 | \tilde{g}_1]\Big] \\ &= \mathbb{E}\Big[\mathbb{I}_{\{\tilde{g}_1 \geq z\}} \mathbb{E}[\tilde{g}_2|\tilde{g}_1]\Big] \\ &= \mathbb{E}\Big[\mathbb{I}_{\{\tilde{g}_1 \geq z\}} \frac{1}{\sqrt{T}} k_1 (\tilde{g}_1^2 - 1)\Big] \\ &= \frac{1}{\sqrt{T}} k_1 \Big(\mathbb{E}[\mathbb{I}_{\{\tilde{g}_1 \geq z\}} \tilde{g}_1^2] - \mathbb{E}[\mathbb{I}_{\{\tilde{g}_1 \geq z\}}]\Big), \end{aligned} \tag{A.15}$$

where $k_1 := g_1\eta\rho n_1 + \frac{1}{2}\sigma_0 f_1 T$, $\eta = \alpha\sqrt{2\kappa}$ and $n_1 = \frac{\kappa T - 1 + e^{-\kappa T}}{T\kappa^2}$.

Simplifying using integration by parts:

$$\begin{aligned}
\mathbb{E}[\mathbb{I}_{\{\tilde{g}_1 \geq z\}}\tilde{g}_1^2] &= \frac{1}{\sqrt{2\pi}}\int_z^\infty x^2 e^{\frac{-x^2}{2}}dx \\
&= \frac{1}{\sqrt{2\pi}}\Big[-xe^{\frac{-x^2}{2}}\Big|_z^\infty + \int_z^\infty e^{\frac{-x^2}{2}}dx\Big] \\
&= \frac{1}{\sqrt{2\pi}}ze^{\frac{-z^2}{2}} + \frac{1}{\sqrt{2\pi}}\int_z^\infty e^{\frac{-x^2}{2}}dx \\
&= z\varphi(z) + \mathbb{E}[\mathbb{I}_{\{\tilde{g}_1 \geq z\}}].
\end{aligned} \tag{A.16}$$

Equation A.15 therefore simplifies to

$$\varphi(z)G_1(z,\hat{\sigma}_0,\hat{\sigma}_1) = \varphi(z)\Big(\frac{1}{2}\sqrt{T}z\hat{\sigma}_0 + \frac{\hat{\sigma}_1}{\hat{\sigma}_0}\Big) = \mathbb{E}[\mathbb{I}_{\{\tilde{g}_1 \geq z\}}\tilde{g}_2] = \frac{1}{\sqrt{T}}k_1 z\varphi(z).$$

Solving for $\hat{\sigma}_1$ and simplifying, the expression for $\hat{\sigma}_1$,

$$\begin{aligned}
\hat{\sigma}_{1,\text{sl}} &= \sigma_0\left(\frac{1}{\sqrt{T}}k_1 - \frac{1}{2}\sqrt{T}\sigma_0\right)z \\
&= \sigma_0\left(\left(\frac{1}{\sqrt{T}}g_1\eta\rho\Big(\frac{\kappa T - 1 + e^{-\kappa T}}{T\kappa^2}\Big) + \frac{1}{2}\sigma_0 f_1 T\right) - \frac{1}{2}\sqrt{T}\sigma_0\right)z \\
&= \frac{\sigma_0 z}{2\sqrt{T}}\left((f_1 - 1)\sigma_0 T + \sqrt{8}g_1\alpha\rho\frac{(\kappa T + e^{\kappa T} - 1)}{T\kappa^{3/2}}\right),
\end{aligned} \tag{A.17}$$

is derived. The subscript sl is used to denote that the implied volatility is for a stochastic and local volatility model. This, along with the local volatility approximation presented in Section 4.2.4 of Kahl (2007), is the result which forms a part of the Watanabe approximation in Jäckel and Kahl (2008).

A similar exercise on (A.14) yields

$$\begin{aligned}
\varphi(z)G_2(z,\hat{\sigma}_0,\hat{\sigma}_1,\hat{\sigma}_2) &= \mathbb{E}\Big[\mathbb{I}_{\{\tilde{g}_1 \geq z\}}\tilde{g}_3 + \frac{1}{2}\delta(\tilde{g}_1 - z)\tilde{g}_2^2\Big] \\
&= \mathbb{E}\Big[\mathbb{E}\Big[\mathbb{I}_{\{\tilde{g}_1 \geq z\}}\tilde{g}_3 + \frac{1}{2}\delta(\tilde{g}_1 - z)\tilde{g}_2^2\Big|\tilde{g}_1\Big]\Big] \\
&= \mathbb{E}\Big[\mathbb{I}_{\{\tilde{g}_1 \geq z\}}\mathbb{E}[\tilde{g}_3|\tilde{g}_1] + \frac{1}{2}\delta(\tilde{g}_1 - z)\mathbb{E}[\tilde{g}_2^2|\tilde{g}_1]\Big] \\
&= \mathbb{E}\Big[\mathbb{I}_{\{\tilde{g}_1 \geq z\}}\mathbb{E}[\tilde{g}_3|\tilde{g}_1]\Big] + \frac{1}{2}\mathbb{E}\Big[\delta(\tilde{g}_1 - z)\mathbb{E}[\tilde{g}_2^2|\tilde{g}_1]\Big],
\end{aligned} \tag{A.18}$$

where expressions for $\mathbb{E}[\tilde{g}_3|\tilde{g}_1]$ and $\mathbb{E}[\tilde{g}_2^2|\tilde{g}_1]$ as functions of $\tilde{g}_1$ are given in Sections 4.2.2.2 and 4.2.2.3 of Kahl (2007). The first expectation contains terms with powers of $\tilde{g}_1^4$, $\tilde{g}_1^3$, $\tilde{g}_1^2$ and $\tilde{g}_1$ due to the expression for $\mathbb{E}[\tilde{g}_3|\tilde{g}_1]$. Integration by parts and the use of the normal probability density function can be used, as demonstrated in

(A.16), to verify the following results:

$$\begin{aligned}
\mathbb{E}[\mathbb{I}_{\{\tilde{g}_1 \geq z\}} \tilde{g}_1] &= \varphi(z), \\
\mathbb{E}[\mathbb{I}_{\{\tilde{g}_1 \geq z\}} \tilde{g}_1^2] &= z\varphi(z) + \mathbb{E}[\mathbb{I}_{\{\tilde{g}_1 \geq z\}}], \\
\mathbb{E}[\mathbb{I}_{\{\tilde{g}_1 \geq z\}} \tilde{g}_1^3] &= (z^2+2)\varphi(z), \\
\mathbb{E}[\mathbb{I}_{\{\tilde{g}_1 \geq z\}} \tilde{g}_1^4] &= z(z^2+3)\varphi(z) + 3\mathbb{E}[\mathbb{I}_{\{\tilde{g}_1 \geq z\}}].
\end{aligned} \tag{A.19}$$

The second expectation in (A.18) can be evaluated by making use of the integral of a Dirac delta function, $\int_{-\infty}^{\infty} \delta(x-z) f(x) dx = f(z)$. One therefore has that, for $\mathbb{E}[\tilde{g}_2^2 | \tilde{g}_1]$ (which is a function of $\tilde{g}_1$),

$$\begin{aligned}
\mathbb{E}\Big[\delta(\tilde{g}_1 - z)\mathbb{E}[\tilde{g}_2^2|\tilde{g}_1]\Big] &= \int_{-\infty}^{\infty} \delta(x-z)\mathbb{E}[\tilde{g}_2^2|\tilde{g}_1]\big|_{\tilde{g}_1=x}\varphi(x)dx, \\
&= \mathbb{E}[\tilde{g}_2^2|\tilde{g}_1]\big|_{\tilde{g}_1=z}\varphi(z).
\end{aligned}$$

Equation A.18 therefore simplifies to

$$\begin{aligned}
\varphi(z)G_2(z,\hat{\sigma}_0,\hat{\sigma}_1,\hat{\sigma}_2) = \varphi(z)\Bigg(&\frac{1}{8}T\hat{\sigma}_0^2 z^4 + \frac{1}{2}\sqrt{T}\hat{\sigma}_1 z^3 - \frac{(T\hat{\sigma}_0^4 - 6\hat{\sigma}_1^2)z^2}{12\hat{\sigma}_0^2} \\
&+ \frac{1}{2}\sqrt{T}\hat{\sigma}_1 z - \frac{T\hat{\sigma}_0^2}{24} + \frac{\hat{\sigma}_2}{\hat{\sigma}_0}\Bigg), \\
= \mathbb{E}\Big[\mathbb{I}_{\{\tilde{g}_1 \geq z\}}\mathbb{E}[\tilde{g}_3|\tilde{g}_1]\Big] &+ \frac{1}{2}\mathbb{E}[\tilde{g}_2^2|\tilde{g}_1]\big|_{\tilde{g}_1=z}\varphi(z),
\end{aligned}$$

where the first expectation is evaluated using the expressions in (A.19). Solving for $\hat{\sigma}_2$ results in

$$\begin{aligned}
\hat{\sigma}_2 = \sigma_0\Bigg[&\frac{1}{2}\mathbb{E}[\tilde{g}_2^2|\tilde{g}_1]\big|_{\tilde{g}_1=z} + \frac{1}{\varphi(z)}\mathbb{E}\Big[\mathbb{I}_{\{\tilde{g}_1 \geq z\}}\mathbb{E}[\tilde{g}_3|\tilde{g}_1]\Big] - \frac{1}{8}T\sigma_0^2 z^4 - \frac{1}{2}\sqrt{T}\hat{\sigma}_1(z^3+z) \\
&+ \frac{T\sigma_0^4 - 6\hat{\sigma}_1^2}{12\sigma_0^2}z^2 + \frac{T\sigma_0^2}{24}\Bigg].
\end{aligned} \tag{A.20}$$

The complexity in simplifying this expression involves algebraic manipulation of the terms $\mathbb{E}[\tilde{g}_2^2|\tilde{g}_1]\big|_{\tilde{g}_1=z}$ and $\mathbb{E}\Big[\mathbb{I}_{\{\tilde{g}_1 \geq z\}}\mathbb{E}[\tilde{g}_3|\tilde{g}_1]\Big]$. The general strategy for recovering the expression presented by Kahl (2007) and used for the Hyp-Hyp model by Jäckel and Kahl (2008) is to compute these conditional expectations and then to match terms according to the order of the polynomial of g_1, g_2 and z or a combination of these. These terms are then manipulated to represent the equivalent terms in the final expression presented by Kahl (2007).

A.2.1 Simplification of $\tilde{g}_3$ Conditional Expectation

Kahl (2007) defines the integrals in the expression for $\tilde{g}_3(T)$ using M_i terms, thus

yielding the expression

$$\tilde{g}_3(T) = \frac{1}{\sqrt{T}}\left(\frac{g_2}{2}M_1 + \sigma_0 g_1 f_1(M_2+M_3) + \sigma_0^2 f_1^2 \int_0^T\int_0^s\int_0^u dW_v dW_u dW_s \right. \\ \left. + \sigma_0^2\frac{f_2}{2}f_0\int_0^T W_s^2 dW_s\right).$$

Noting that, as given in Kahl (2007),

$$\mathbb{E}\Big[\int_0^T\int_0^s\int_0^u dW_v dW_u dW_s\Big|\tilde{g}_1\Big] = \frac{\tilde{g}_1(\tilde{g}_1^2-3)T^{3/2}}{6},$$

and that

$$\mathbb{E}\Big[\int_0^T W_s^2 dW_s\Big|\tilde{g}_1\Big] = \frac{1}{3}\tilde{g}_1^3 T^{3/2} - \frac{1}{2}\tilde{g}_1 T^{3/2},$$

and defining the other conditional expectations as $m_i(\tilde{g}_1\sqrt{T}) := \mathbb{E}[M_i|\tilde{g}_1]$, one can see that

$$\mathbb{E}\Big[\mathbb{I}_{\{\tilde{g}_1\geq z\}}\mathbb{E}[\tilde{g}_3|\tilde{g}_1]\Big] = \mathbb{E}\Bigg[\mathbb{I}_{\{\tilde{g}_1\geq z\}}\frac{1}{\sqrt{T}}\Bigg(\frac{g_2}{2}m_1(\tilde{g}_1\sqrt{T}) + \sigma_0 g_1 f_1(m_2(\tilde{g}_1\sqrt{T}) \\ + m_3(\tilde{g}_1\sqrt{T})) + \sigma_0^2 f_1^2\frac{\tilde{g}_1(\tilde{g}_1^2-3)T^{3/2}}{6} + \sigma_0^2\frac{f_2}{2}f_0\left(\frac{1}{3}\tilde{g}_1^3T^{3/2} - \frac{1}{2}\tilde{g}_1T^{3/2}\right)\Bigg)\Bigg]. \tag{A.21}$$

Rearranging the expression for $m_1(\tilde{g}_1\sqrt{T})$ given by Kahl (2007) yields

$$m_1(\tilde{g}_1\sqrt{T}) = \eta^2\rho^2\frac{e^{-2T\kappa}}{4T^3\kappa^3}T^{3/2}\Big[(-2+8e^{T\kappa}+e^{2T\kappa}(4T\kappa-6))\tilde{g}_1^3 \\ + (-24e^{T\kappa}+6+T\kappa+e^{2T\kappa}(T\kappa-2)(2T\kappa-9))\tilde{g}_1\Big] =: A\tilde{g}_1^3 + B\tilde{g}_1,$$

where A and B represent the coefficients of $\tilde{g}_1^3$ and $\tilde{g}_1$ defined above.

As in Section 4.2.2.1 of Kahl (2007), the integral M_1 can be decorrelated. The SDE describing the dynamics of y_t are

$$dy_t = -\kappa y_t dt + \alpha\sqrt{2\kappa}dZ_t$$

and the solution to this SDE is

$$y_t = \alpha\sqrt{2\kappa}\int_0^t e^{-\kappa(t-s)}dZ_s = \eta\int_0^t e^{-\kappa(t-s)}dZ_s.$$

Evaluating the integral of M_1 results in

$$M_1 = \int_0^T y_t^2 dW_t \\ = \int_0^T\left(\eta\int_0^t e^{-\kappa(t-u)}dZ_u\right)^2 dW_t,$$

which has the conditional expectation

$$\begin{aligned}\mathbb{E}[M_1|\tilde{g}_1] &= \eta^2\mathbb{E}\left[\int_0^T\left(e^{-\kappa t}\int_0^t e^{\kappa u}dZ_u\right)^2 dW_t\middle|\tilde{g}_1\right] \\ &= \eta^2\mathbb{E}\left[\int_0^T\left(\rho e^{-\kappa t}\int_0^t e^{\kappa u}dW_u + \sqrt{1-\rho^2}e^{-\kappa t}\int_0^t e^{\kappa u}d\hat{Z}_u\right)^2 dW_t\middle|\tilde{g}_1\right],\end{aligned}$$

where $\hat{Z}_t$ is uncorrelated with W_t. The above result is attained from a Cholesky decomposition of the Brownian motion Z_t. The cross term (that is, the middle term of the polynomial which contains an integral with respect to $\hat{Z}_t$) has an expectation of 0 when conditioned on $\tilde{g}_1 := W_t/\sqrt{t}$. The final term in the polynomial is, by Itô isometry,

$$\left(\sqrt{1-\rho^2}e^{-\kappa T}\int_0^t e^{\kappa u}d\hat{Z}_u\right)^2 = e^{-2\kappa T}(1-\rho^2)\int_0^t e^{2\kappa u}du = \frac{1}{2}(1-\rho^2)(1-e^{-2\kappa t}),$$

which is a finite variation process and thus becomes zeros when integrated by dW_t.

We thus have the result for Lemma 4.21 in Kahl (2007):

$$\mathbb{E}[M_1|\tilde{g}_1] = \eta^2\rho^2\mathbb{E}\left[\int_0^T\left(e^{-\kappa t}\int_0^t e^{\kappa u}dW_u\right)^2 dW_t\middle|\tilde{g}_1\right] = m_1(\tilde{g}_1\sqrt{T}).$$

The expression for the conditional expectation is given by

$$\eta^2\rho^2\mathbb{E}\left[\int_0^T\left(e^{-\kappa t}\int_0^t e^{\kappa u}dW_u\right)^2 dW_t\middle|\tilde{g}_1\right] = A\tilde{g}_1^3 + B\tilde{g}_1.$$

and can be combined with the expressions given in (A.19), to yield the result

$$\sigma_0 \frac{1}{\varphi(z)} \mathbb{E}\Big[\mathbb{I}_{\{\tilde{g}_1 \geq z\}} \frac{1}{\sqrt{T}} \frac{g_2}{2} m_1(\tilde{g}_1\sqrt{T})\Big] \tag{A.22}$$

$$\begin{aligned}
&= \sigma_0 \frac{1}{\sqrt{T}} \frac{g_2}{2} \big(A(z^2+2)+B\big) \\
&= \eta^2\rho^2\sigma_0 \frac{g_2}{2} \frac{e^{-2T\kappa}}{4T^3\kappa^3} T\Big[\big(-2+8e^{T\kappa}+e^{2T\kappa}(4T\kappa-6)\big)(z^2+2) \\
&\quad -24e^{T\kappa}+6+T\kappa+2e^{2T\kappa}T^2\kappa^2-13e^{2T\kappa}T\kappa+18e^{2T\kappa}\Big] \\
&= \eta^2\rho^2\sigma_0 \frac{g_2}{2} \frac{e^{-2T\kappa}}{4T^3\kappa^3} T\Big[-2z^2+8e^{T\kappa}z^2+e^{2T\kappa}(4T\kappa-6)z^2 \\
&\qquad -4+16e^{T\kappa}+8e^{2T\kappa}T\kappa-12e^{2T\kappa} \\
&\quad -24e^{T\kappa}+6+T\kappa+2e^{2T\kappa}T^2\kappa^2-13e^{2T\kappa}T\kappa+18e^{2T\kappa}\Big] \\
&= 2\eta^2\rho^2\sigma_0\alpha^2\kappa\rho^2 \frac{g_2}{2} \frac{e^{-2T\kappa}}{4T^3\kappa^3} T\Big[(2e^{2T\kappa}T^2\kappa^2-5e^{2T\kappa}T\kappa+T\kappa \\
&\quad -8e^{T\kappa}+6e^{2T\kappa}+2)+(4e^{2T\kappa}T\kappa+8e^{T\kappa}-6e^{2T\kappa}-2)z^2\Big] \\
&= \sigma_0 \frac{e^{-2T\kappa}}{24T^3\kappa^3} T\kappa\Big[6g_2\alpha^2(2e^{2T\kappa}T^2\kappa^2-5e^{2T\kappa}T\kappa+T\kappa \\
&\qquad\qquad -8e^{T\kappa}+6e^{2T\kappa}+2) \\
&\qquad +6g_2(4e^{2T\kappa}T\kappa+8e^{T\kappa}-6e^{2T\kappa}-2)\rho^2z^2\Big].
\end{aligned} \tag{A.23}$$

The result of (A.23) above agrees with the terms containing g_2 in the $\hat{\sigma}_2$ term presented in Jäckel and Kahl (2008).

The expressions for $m_2(\tilde{g}_1\sqrt{T})$ and $m_3(\tilde{g}_1\sqrt{T})$ are summed and rearranged to give

$$\begin{aligned}
m_2(\tilde{g}_1\sqrt{T})+m_3(\tilde{g}_1\sqrt{T}) &= \eta\rho \frac{1}{2T^3\kappa^3}\Big[\tilde{g}_1\sqrt{T}e^{-T\kappa}((\tilde{g}_1\sqrt{T})^2(2T\kappa+e^{T\kappa}(T^2\kappa^2-2) \\
&\qquad +2)-T(4T\kappa+e^{T\kappa}(T\kappa(T\kappa+2)-6)+6)) \\
&\qquad +\tilde{g}_1\sqrt{T}((\tilde{g}_1\sqrt{T})^2-3T)(T\kappa(T\kappa-2)-2e^{T\kappa}+2)\Big] \\
&= \frac{1}{2T^3\kappa^3}T^{3/2}\Big[(2T^2\kappa^2-2T\kappa+2T\kappa e^{-T\kappa})\tilde{g}_1^3 \\
&\qquad -(2T^2\kappa^2-2T\kappa+2T\kappa e^{-T\kappa})\tilde{g}_1\Big] \\
&= n_1\sqrt{T}(\tilde{g}_1^3-2\tilde{g}_1),
\end{aligned}$$

where n_1 is as defined before. In a similar manner to the decorrelation step done with regards to the integral given by M_1, η and ρ are incorporated into the expres-

sion. We therefore have

$$\begin{aligned}
&\sigma_0 \frac{1}{\varphi(z)} \mathbb{E}\Big[\mathbb{I}_{\{\tilde{g}_1 \geq z\}} \frac{1}{\sqrt{T}} \sigma_0 g_1 f_1 n_1 \sqrt{T}(\tilde{g}_1^3 - 2\tilde{g}_1)\Big] \\
&\qquad = \sigma_0 \frac{1}{\varphi(z)} \eta\rho \mathbb{E}\Big[\mathbb{I}_{\{\tilde{g}_1 \geq z\}} \sigma_0 g_1 f_1 n_1 (\tilde{g}_1^3 - 2\tilde{g}_1)\Big] \\
&\qquad = \sigma_0 \frac{1}{\varphi(z)} \alpha\sqrt{2\kappa}\rho\sigma_0 g_1 f_1 n_1 \big((z^2+2)\varphi(z) - 2\varphi(z)\big) \\
&\qquad = \sigma_0^2 \alpha\sqrt{2\kappa}\rho g_1 f_1 n_1 z^2 \\
&\qquad = \sigma_0^2 \alpha\sqrt{2\kappa}\rho g_1 f_1 \frac{(T\kappa - 1 + e^{-T\kappa})}{T\kappa^2} z^2 \\
&\qquad = \frac{\sigma_0^2 e^{-2T\kappa}}{24T^3\kappa^3} \Big[24 e^{T\kappa} \alpha\sqrt{2\kappa}\rho g_1 f_1 (e^{T\kappa}(T\kappa - 1) + 1) T^2 \kappa z^2\Big] \\
&\qquad = \frac{\sigma_0 e^{-2T\kappa}}{24T^3\kappa^3} \Big[12\sqrt{2} e^{T\kappa} g_1 f_1 \alpha \kappa^{3/2} (e^{T\kappa}(T\kappa - 1) + 1) \rho\sigma_0 T^2 (2z^2)\Big],
\end{aligned} \tag{A.24}$$

A.2.2 Simplification of $\tilde{g}_2^2$ Conditional Expectation

Kahl (2007) gives the expression

$$\mathbb{E}[\tilde{g}_2^2 | \tilde{g}_1] = \frac{1}{T}\Big(k_1^2(\tilde{g}_1^4 - 2\tilde{g}_1^2 + 1) + g_1^2\eta^2(1-\rho^2) n_{(2,2)}\big(\tilde{g}_1\sqrt{T}\big)\Big)$$

where

$$\begin{aligned}
n_{(2,2)}(\tilde{g}_1\sqrt{T}) = \frac{e^{-2T\kappa}}{4T^2\kappa^3} \big((e^{2T\kappa}(4T\kappa - 6) + 8e^{T\kappa} - 2)(\tilde{g}_1\sqrt{T})^2 + \\
T(T\kappa - 8e^{T\kappa} + e^{2T\kappa}(T\kappa(2T\kappa - 5) + 6) + 2)\big).
\end{aligned}$$

We therefore have that

$$\frac{1}{2}\mathbb{E}[\tilde{g}_2^2 | \tilde{g}_1]\big|_{\tilde{g}_1 = z} = \frac{1}{2T}\Big(k_1^2(z^4 - 2z^2 + 1) + g_1^2\eta^2(1-\rho^2) n_{(2,2)}\big(z\sqrt{T}\big)\Big) \tag{A.25}$$

Considering the z^4 term of first term in (A.25), and grouping this with the other terms containing z^4 from (A.20) results in

$$\begin{aligned}
&\frac{1}{2T}k_1^2 z^4 - \frac{1}{8}T\sigma_0^2 z^4 - \frac{1}{2}\sqrt{T}\hat{\sigma}_1 z^3 - \frac{1}{2}\frac{\hat{\sigma}_1^2}{\sigma_0^2} z^2 \\
&= \frac{1}{2T}k_1^2 z^4 - \frac{1}{8}T\sigma_0^2 z^4 - \frac{1}{2}\sqrt{T}\sigma_0\left(\frac{1}{\sqrt{T}}k_1 - \frac{1}{2}\sqrt{T}\sigma_0\right) z^4 - \frac{1}{2}\left(\frac{1}{\sqrt{T}}k_1 - \frac{1}{2}\sqrt{T}\sigma_0\right)^2 z^4 \\
&= \frac{1}{2T}k_1^2 z^4 - \frac{1}{8}T\sigma_0^2 z^4 - \frac{1}{2}\sigma_0 k_1 z^4 + \frac{1}{4}T\sigma_0^2 z^4 - \frac{1}{2T}k_1^2 z^4 + \frac{1}{2}k_1\sigma_0 z^4 - \frac{1}{8}T\sigma_0^2 z^4 = 0.
\end{aligned}$$

Different powers of g_1 appear in the remainder of the k_1^2 term:

$$\frac{1}{2T}k_1^2(1 - 2z^2) = \frac{1}{2T}\Big(g_1^2\eta^2\rho^2 n_1^2 + \sigma_0 T g_1 f_1 \eta\rho n_1 + \frac{1}{4}T^2 f_1^2 \sigma_0^2\Big)(1 - 2z^2). \tag{A.26}$$

Grouping the middle term in this expression with a term containing a z^2 and g_1 (from the $\hat{\sigma}_1$) from (A.20) results in

$$\begin{aligned}
&\sigma_0\Big(-\frac{1}{2}\sqrt{T}\hat{\sigma}_1 z+\frac{(1-2z^2)\sigma_0 T g_1 f_1\eta\rho n_1}{2T}\Big)\\
&=-\frac{\sigma_0}{2}\sigma_0 g_1\eta\rho n_1 z^2-\frac{1}{2}\sqrt{T}\frac{\sigma_0^3}{2}\sqrt{T}(f_1-1)z^2+\frac{\sigma_0 g_1 f_1\eta\rho n_1}{2}(1-2z^2)\\
&=\frac{\sigma_0}{2}(-g_1z^2+g_1f_1-2g_1f_1z^2)\sigma_0\eta\rho n_1-\frac{1}{4}Tz^2(f_1-1)\sigma_0^3\\
&=\frac{\sigma_0}{2}(-g_1z^2+g_1f_1-2g_1f_1z^2)\sigma_0\alpha\sqrt{2\kappa}\rho\frac{\kappa T-1+e^{-\kappa T}}{T\kappa^2}-\frac{1}{4}Tz^2(f_1-1)\sigma_0^3\\
&=\frac{\sigma_0 e^{-2T\kappa}}{24T^3\kappa^3}\Big[12\sqrt{2}e^{T\kappa}\alpha\kappa^{3/2}(e^{T\kappa}(T\kappa-1)+1)\rho\sigma_0T^2(-g_1z^2+g_1f_1-2g_1f_1z^2)\Big]\\
&-\frac{1}{4}Tz^2(f_1-1)\sigma_0^3. \qquad \text{(A.27)}
\end{aligned}$$

If one combines (A.24) and the first term of (A.27), one gets

$$\begin{aligned}
&\frac{\sigma_0 e^{-2T\kappa}}{24T^3\kappa^3}\Big[12\sqrt{2}e^{T\kappa}g_1f_1\alpha\kappa^{3/2}(e^{T\kappa}(T\kappa-1)+1)\rho\sigma_0T^2(2z^2)\Big]\\
&+\frac{\sigma_0 e^{-2T\kappa}}{24T^3\kappa^3}\Big[12\sqrt{2}e^{T\kappa}\alpha\kappa^{3/2}(e^{T\kappa}(T\kappa-1)+1)\rho\sigma_0T^2(-g_1z^2+g_1f_1-2g_1f_1z^2)\Big]\\
&=\frac{\sigma_0 e^{-2T\kappa}}{24T^3\kappa^3}\Big[12\sqrt{2}e^{T\kappa}g_1f_1\alpha\kappa^{3/2}(e^{T\kappa}(T\kappa-1)+1)\rho\sigma_0T^2\Big]\\
&\qquad+\frac{\sigma_0 e^{-2T\kappa}}{24T^3\kappa^3}\Big[-12\sqrt{2}e^{T\kappa}g_1\alpha\kappa^{3/2}(e^{T\kappa}(T\kappa-1)+1)\rho\sigma_0T^2z^2\Big], \qquad \text{(A.28)}
\end{aligned}$$

which forms part of the approximation given in Jäckel and Kahl (2008).

Grouping terms from (A.20), (A.21) and (A.26) which have no terms containing g_1 or g_2 and using the expectations defined in (A.19) results in

$$\begin{aligned}
&\sigma_0\frac{1}{\varphi(z)}\mathbb{E}\left[\mathbb{I}_{\{\tilde{g}_1\geq z\}}\frac{1}{\sqrt{T}}\sigma_0^2f_1^2\frac{\tilde{g}_1(\tilde{g}_1^2-3)T^{3/2}}{6}\right]+\frac{T\sigma_0^2}{12}z^2+\frac{T\sigma_0^2}{24}+\frac{\sigma_0^2T}{8}f_1^2(1-2z^2)\\
&\qquad=\sigma_0\left(\frac{1}{6}Tf_1^2\sigma_0^2\frac{1}{\varphi(z)}\mathbb{E}[\mathbb{I}_{\{\tilde{g}_1\geq z\}}(\tilde{g}_1^3-3\tilde{g}_1)]\right.\\
&\qquad\qquad\left.+\frac{T\sigma_0^2}{12}z^2+\frac{T\sigma_0^2}{24}+\frac{\sigma_0^2Tf_1^2}{8}-\frac{\sigma_0^2Tf_1^2}{4}z^2\right)\\
&\qquad=\sigma_0\left(\frac{1}{6}Tf_1^2\sigma_0^2((z^2+2)-3)+\frac{T\sigma_0^2}{12}z^2+\frac{T\sigma_0^2}{24}+\frac{\sigma_0^2Tf_1^2}{8}-\frac{\sigma_0^2Tf_1^2}{4}z^2\right)\\
&\qquad=\sigma_0\left(-\frac{1}{12}f_1^2\sigma_0^2Tz^2-\frac{1}{24}f_1^2\sigma_0^2T+\frac{1}{12}\sigma_0^2Tz^2+\frac{1}{24}\sigma_0^2T\right)\\
&\qquad=\frac{\sigma_0e^{-2T\kappa}}{24T^3\kappa^3}T\kappa\Big(-e^{2T\kappa}(f_1^2-1)T^3\kappa^2\sigma_0^2\Big)\\
&\qquad\qquad+\frac{\sigma_0e^{-2T\kappa}}{24T^3\kappa^3}T\kappa\Big(-e^{2T\kappa}(2f_1^2-2)T^3\kappa^2\sigma_0^2\Big)z^2, \qquad \text{(A.29)}
\end{aligned}$$

Simplifying the last term in (A.21) yields the result

$$\begin{aligned}
&\sigma_0 \frac{1}{\varphi(z)} \mathbb{E}\left[\mathbb{I}_{\{\tilde{g}_1 \geq z\}} \frac{1}{\sqrt{T}} \left(\sigma_0^2 \frac{f_2}{2} f_0 \left(\frac{1}{3}\tilde{g}_1^3 T^{3/2} - \frac{1}{2}\tilde{g}_1 T^{3/2}\right)\right)\right] \\
&\quad = \frac{\sigma_0^3 T f_2}{2\varphi(z)} \left(\frac{1}{3}\mathbb{E}[\mathbb{I}_{\{\tilde{g}_1 \geq z\}}\tilde{g}_1^3] - \frac{1}{2}\mathbb{E}[\mathbb{I}_{\{\tilde{g}_1 \geq z\}}\tilde{g}_1]\right) \\
&\quad = \frac{\sigma_0^3 T f_2}{2\varphi(z)} \left(\frac{1}{3}\varphi(z)(z^2+2) - \frac{1}{2}\varphi(z)\right) \\
&\quad = \frac{\sigma_0^3 T f_2}{2} \left(\frac{1}{3}z^2 + \frac{6}{2}\right) \\
&\quad = \frac{\sigma_0 e^{-2T\kappa} T\kappa}{24T^3\kappa^3} \left(- e^{2T\kappa}(-4f_2 z^2 - 2f_2) T^3\kappa^2\sigma_0^2\right). \qquad \text{(A.30)}
\end{aligned}$$

The final term in (A.27) can be expanded to

$$-\frac{1}{4}Tz^2(f_1-1)\sigma_0^3 = \frac{\sigma_0 e^{-2T\kappa}}{24T^3\kappa^3} T\kappa \left(- e^{2T\kappa}(6f_1 - 6) T^3\kappa^2\sigma_0^2\right) z^2, \qquad \text{(A.31)}$$

Combining (A.29), (A.30) and (A.31) results in

$$\begin{aligned}
&\frac{\sigma_0 e^{-2T\kappa}}{24T^3\kappa^3} T\kappa \Big(- e^{2T\kappa}(f_1^2 - 1) T^3\kappa^2\sigma_0^2\Big) + \frac{\sigma_0 e^{-2T\kappa}}{24T^3\kappa^3} T\kappa \Big(- e^{2T\kappa}(2f_1^2 - 2) T^3\kappa^2\sigma_0^2\Big) z^2 \\
&+ \frac{\sigma_0 e^{-2T\kappa} T\kappa}{24T^3\kappa^3} \Big(- e^{2T\kappa}(-4f_2 z^2 - 2f_2) T^3\kappa^2\sigma_0^2\Big) \\
&\qquad + \frac{\sigma_0 e^{-2T\kappa}}{24T^3\kappa^3} T\kappa \Big(- e^{2T\kappa}(6f_1 - 6) T^3\kappa^2\sigma_0^2\Big) z^2 \\
&= \frac{\sigma_0 e^{-2T\kappa}}{24T^3\kappa^3} T\kappa \Big(- e^{2T\kappa}(f_1^2 - 2f_2 - 1) T^3\kappa^2\sigma_0^2\Big) \\
&\qquad + \frac{\sigma_0 e^{-2T\kappa}}{24T^3\kappa^3} T\kappa \Big(- e^{2T\kappa}(2f_1^2 + 6f_1 - 4f_2 - 8) T^3\kappa^2\sigma_0^2\Big) z^2, \qquad \text{(A.32)}
\end{aligned}$$

which is identical to the corresponding terms in the approximation given by Jäckel and Kahl (2008).

Lastly, considering the terms from (A.25) and (A.26) which contain g_1^2, one has

$$\begin{aligned}
&\sigma_0 \frac{1}{2T}\Big(g_1^2\eta^2\rho^2 n_1^2(1-2z^2) + g_1^2\eta^2(1-\rho^2) n_{(2,2)}\big(z\sqrt{T}\big)\Big) \\
&= \sigma_0 \frac{1}{2T} g_1^2\eta^2 \Big(\rho^2 \Big(\frac{\kappa T - 1 + e^{-\kappa T}}{T\kappa^2}\Big)^2 (1-2z^2) \\
&\quad + (1-\rho^2)\frac{e^{-2T\kappa}}{4T^2\kappa^3}\big(T(e^{2T\kappa}(4T\kappa - 6) + 8e^{T\kappa} - 2)z^2 \\
&\qquad + T(T\kappa - 8e^{T\kappa} + e^{2T\kappa}(T\kappa(2T\kappa - 5) + 6) + 2)\big)\Big) \\
&= \sigma_0 \frac{e^{-2T\kappa}}{4T^3\kappa^3} g_1^2\alpha^2\kappa \Big(4e^{2T\kappa}\rho^2 \frac{(\kappa T - 1 + e^{-\kappa T})^2}{\kappa}(1-2z^2)
\end{aligned}$$

$$
\begin{aligned}
&+ (1-\rho^2)\big(T(e^{2T\kappa}(4T\kappa-6)+8e^{T\kappa}-2)z^2 \\
&\quad + T(T\kappa - 8e^{T\kappa} + e^{2T\kappa}(T\kappa(2T\kappa-5)+6)+2)\big)\Big) \\
&= \sigma_0 \frac{e^{-2T\kappa}}{4T^3\kappa^3} g_1^2\alpha^2\Big(4\rho^2\Big((e^{\kappa T}-1)^2 + 2e^{T\kappa}T\kappa - 2e^{2T\kappa}T\kappa \\
&\quad + e^{2T\kappa}\kappa^2T^2\Big)(1-2z^2) \\
&\quad + (1-\rho^2)\big(T\kappa(e^{2T\kappa}(4T\kappa-6)+8e^{T\kappa}-2)z^2 \\
&\quad + T\kappa(T\kappa - 8e^{T\kappa} + e^{2T\kappa}(T\kappa(2T\kappa-5)+6)+2)\big)\Big) \\
&= \sigma_0 \frac{e^{-2T\kappa}}{4T^3\kappa^3} g_1^2\alpha^2\Big(4\rho^2\Big((e^{\kappa T}-1)^2 + 2e^{T\kappa}T\kappa - 2e^{2T\kappa}T\kappa \\
&\quad + e^{2T\kappa}\kappa^2T^2\Big)(1-2z^2) \\
&\quad + (1-\rho^2)\big((4e^{2T\kappa}T^2\kappa^2 - 6e^{2T\kappa}T\kappa + 8e^{T\kappa}T\kappa - 2T\kappa)z^2 \\
&\quad + T^2\kappa^2 - 8e^{T\kappa}T\kappa + 2e^{2T\kappa}T^3\kappa^3 - 5e^{2T\kappa}T^2\kappa^2 + 6e^{2T\kappa}T\kappa + 2T\kappa\big)\Big) \\
&= \sigma_0 \frac{e^{-2T\kappa}}{4T^3\kappa^3} g_1^2\alpha^2\Big(4\rho^2(e^{\kappa T}-1)^2 + 8\rho^2e^{T\kappa}T\kappa - 8\rho^2e^{2T\kappa}T\kappa + 4\rho^2e^{2T\kappa}\kappa^2T^2 \\
&- 8\rho^2(e^{\kappa T}-1)^2z^2 - 16\rho^2e^{T\kappa}T\kappa z^2 + 16\rho^2e^{2T\kappa}T\kappa z^2 - 8\rho^2e^{2T\kappa}T^2\kappa^2z^2 \\
&\quad + 4e^{2T\kappa}T^2z^2\kappa^2 - 6e^{2T\kappa}T\kappa z^2 + 8e^{T\kappa}T\kappa z^2 - 2T\kappa z^2 \\
&\quad - 4e^{2T\kappa}T^2\rho^2z^2\kappa^2 + 6e^{2T\kappa}T\kappa\rho^2z^2 - 8e^{T\kappa}T\kappa\rho^2z^2 + 2T\kappa\rho^2z^2 \\
&\quad + T^2\kappa^2 - 8e^{T\kappa}T\kappa + 2e^{2T\kappa}T^3\kappa^3(1-\rho^2) - 5e^{2T\kappa}T^2\kappa^2 + 6e^{2T\kappa}T\kappa + 2T\kappa \\
&\quad - T^2\kappa^2\rho^2 + 8e^{T\kappa}T\kappa\rho^2 + 5e^{2T\kappa}T^2\kappa^2\rho^2 - 6e^{2T\kappa}T\kappa\rho^2 - 2T\kappa\rho^2\Big) \\
&= \sigma_0 \frac{e^{-2T\kappa}}{4T^3\kappa^3} g_1^2\alpha^2\Big(\big(4\rho^2(e^{\kappa T}-1)^2 + 8\rho^2e^{T\kappa}T\kappa - 8\rho^2e^{2T\kappa}T\kappa + 4\rho^2e^{2T\kappa}\kappa^2T^2 \\
&\quad + T^2\kappa^2 - 8e^{T\kappa}T\kappa + 2e^{2T\kappa}T^3\kappa^3(1-\rho^2) - 5e^{2T\kappa}T^2\kappa^2 + 6e^{2T\kappa}T\kappa + 2T\kappa \\
&\quad - T^2\kappa^2\rho^2 + 8e^{T\kappa}T\kappa\rho^2 + 5e^{2T\kappa}T^2\kappa^2\rho^2 - 6e^{2T\kappa}T\kappa\rho^2 - 2T\kappa\rho^2\big) + \\
&\quad \big(-8\rho^2(e^{\kappa T}-1)^2 - 16\rho^2e^{T\kappa}T\kappa + 16\rho^2e^{2T\kappa}T\kappa - 8\rho^2e^{2T\kappa}T^2\kappa^2 \\
&\quad + 4e^{2T\kappa}T^2\kappa^2 - 6e^{2T\kappa}T\kappa + 8e^{T\kappa}T\kappa - 2T\kappa - 4e^{2T\kappa}T^2\rho^2\kappa^2 \\
&\quad\quad + 6e^{2T\kappa}T\kappa\rho^2 - 8e^{T\kappa}T\kappa\rho^2 + 2T\kappa\rho^2\big)z^2\Big) \\
&= \sigma_0 \frac{e^{-2T\kappa}}{4T^3\kappa^3} g_1^2\alpha^2\Big(\big(-2e^{2T\kappa}T^3\kappa^3(\rho^2-1) + (4\rho^2e^{2T\kappa}+1 \\
&\quad\quad - 5e^{2T\kappa} + 5e^{2T\kappa}\rho^2 - \rho^2)T^2\kappa^2 + (8\rho^2e^{T\kappa} - 8\rho^2e^{2T\kappa} - 8e^{T\kappa} + 6e^{2T\kappa} + 2 \\
&\quad + 8e^{T\kappa}\rho^2 - 6e^{2T\kappa}\rho^2 - 2\rho^2)T\kappa + 4\rho^2(e^{\kappa T}-1)^2\big) + \\
&\quad \big((-8\rho^2e^{2T\kappa} + 4e^{2T\kappa} - 4e^{2T\kappa}\rho^2)T^2\kappa^2 - 8\rho^2(e^{\kappa T}-1)^2 \\
&\quad + (-16\rho^2e^{T\kappa} + 16\rho^2e^{2T\kappa} - 6e^{2T\kappa} + 8e^{T\kappa} - 2 \\
&\quad\quad + 6e^{2T\kappa}\rho^2 - 8e^{T\kappa}\rho^2 + 2\rho^2)T\kappa\big)z^2\Big) \\
&= \sigma_0 \frac{e^{-2T\kappa}}{4T^3\kappa^3} g_1^2\alpha^2\Big(\big(-2e^{2T\kappa}T^3\kappa^3(\rho^2-1) + (9\rho^2e^{2T\kappa} - \rho^2 - 5e^{2T\kappa} + 1)T^2\kappa^2
\end{aligned}
$$

$$
\begin{aligned}
&+ (16\rho^2 e^{T\kappa} - 8e^{T\kappa} + 6e^{2T\kappa} - 14e^{2T\kappa}\rho^2 + 2 - 2\rho^2)T\kappa \\
&+ 4\rho^2(e^{\kappa T} - 1)^2) + \big((-12\rho^2 e^{2T\kappa} + 4e^{2T\kappa})T^2\kappa^2 \\
&- 8\rho^2(e^{\kappa T} - 1)^2 + (-24\rho^2 e^{T\kappa} + 22\rho^2 e^{2T\kappa} - 6e^{2T\kappa} + 8e^{T\kappa} - 2 \\
&+ 2\rho^2)T\kappa\big)z^2\Big) \\
= \sigma_0 \frac{e^{-2T\kappa}}{4T^3\kappa^3} g_1^2\alpha^2\Big(&(- 2e^{2T\kappa}T^3\kappa^3(\rho^2 - 1) + (9\rho^2 e^{2T\kappa} - \rho^2 - 5e^{2T\kappa} + 1)T^2\kappa^2 \\
&+ (14\rho^2 e^{T\kappa} + 2\rho^2 e^{T\kappa} - 6e^{T\kappa} - 2e^{T\kappa} + 6e^{2T\kappa} - 14e^{2T\kappa}\rho^2 + 2 - 2\rho^2)T\kappa \\
&+ 4\rho^2(e^{\kappa T} - 1)^2\rho^2) + \big((-12\rho^2 e^{2T\kappa} + 4e^{2T\kappa})T^2\kappa^2 \\
&- 8\rho^2(e^{\kappa T} - 1)^2 + (-22\rho^2 e^{T\kappa} - 2\rho^2 e^{T\kappa} + 22\rho^2 e^{2T\kappa} - 6e^{2T\kappa} + \\
&6e^{T\kappa} + 2e^{T\kappa} - 2 + 2\rho^2)T\kappa\big)z^2\Big) \\
= \sigma_0 \frac{e^{-2T\kappa}}{4T^3\kappa^3} g_1^2\alpha^2\Big(&(- 2e^{2T\kappa}T^3\kappa^3(\rho^2 - 1) + (9\rho^2 e^{2T\kappa} - \rho^2 - 5e^{2T\kappa} + 1)T^2\kappa^2 \\
&+ (-14(e^{T\kappa} - 1)\rho^2 e^{T\kappa} + 2(e^{T\kappa} - 1)\rho^2 - 2(e^{T\kappa} - 1) + 6(e^{T\kappa} - 1)e^{T\kappa})T\kappa \\
&+ 4\rho^2(e^{\kappa T} - 1)^2) + \big((-12\rho^2 e^{2T\kappa} + 4e^{2T\kappa})T^2\kappa^2 \\
&- 8\rho^2(e^{\kappa T} - 1)^2 + (22(e^{T\kappa} - 1)\rho^2 e^{T\kappa} - 2(e^{T\kappa} - 1)\rho^2 \\
&+ 2(e^{T\kappa} - 1) - 6(e^{T\kappa} - 1)e^{T\kappa})T\kappa\big)z^2\Big) \\
= -\sigma_0 \frac{e^{-2T\kappa}}{24T^3\kappa^3} 6g_1^2\alpha^2\Big(&\big(2e^{2T\kappa}T^3\kappa^3(\rho^2 - 1) + (-9\rho^2 e^{2T\kappa} + \rho^2 + 5e^{2T\kappa} - 1)T^2\kappa^2 \\
&- 2(e^{T\kappa} - 1)(-7\rho^2 e^{T\kappa} + \rho^2 + 3e^{T\kappa} - 1)T\kappa \\
&- 4\rho^2(e^{\kappa T} - 1)^2\big) + \big((12\rho^2 e^{2T\kappa} - 4e^{2T\kappa})T^2\kappa^2 \\
&+ 8\rho^2(e^{\kappa T} - 1)^2 - 2(e^{T\kappa} - 1)(11\rho^2 e^{T\kappa} - \rho^2 - 3e^{T\kappa} + 1)T\kappa\big)z^2\Big), \qquad \text{(A.33)}
\end{aligned}
$$

which is identical to the terms containing g_1^2 in the approximation used in Jäckel and Kahl (2008).

Combining the results from (A.23), (A.28), (A.32) and (A.33) with the expression (A.20) would yield

$$
\begin{aligned}
\hat{\sigma}_{2,\text{sl}} = \sigma_0 \frac{e^{-2T\kappa}}{24T^3\kappa^3} T\kappa\Big[&6g_2\alpha^2(2e^{2T\kappa}T^2\kappa^2 - 5e^{2T\kappa}T\kappa + T\kappa - 8e^{T\kappa} + 6e^{2T\kappa}) \\
&+ 6g_2(4e^{2T\kappa}T\kappa + 8e^{T\kappa} - 6e^{2T\kappa} - 2)\rho^2 z^2\Big] \\
&+ \sigma_0 \frac{e^{-2T\kappa}}{24T^3\kappa^3}\Big[12\sqrt{2}e^{T\kappa} f_1 g_1 \alpha\kappa^{3/2}(e^{T\kappa}(T\kappa - 1) + 1)\rho\sigma_0 T^2(1 - z^2)\Big] \\
&- \sigma_0 \frac{e^{-2T\kappa}}{24T^3\kappa^3} 6g_1^2\alpha^2\Big[\big(2e^{2T\kappa}T^3\kappa^3(\rho^2 - 1) + (-9\rho^2 e^{2T\kappa} + \rho^2 \\
&+ 5e^{2T\kappa} - 1)T^2\kappa^2 - 2(e^{T\kappa} - 1)(-7\rho^2 e^{T\kappa} + \rho^2 + 3e^{T\kappa} - 1)T\kappa \\
&- 4\rho^2(e^{\kappa T} - 1)^2\big) + \big((12\rho^2 e^{2T\kappa} - 4e^{2T\kappa})T^2\kappa^2 \\
&+ 8\rho^2(e^{\kappa T} - 1)^2 - 2(e^{T\kappa} - 1)(11\rho^2 e^{T\kappa} - \rho^2 - 3e^{T\kappa} + 1)T\kappa\big)z^2\Big]
\end{aligned}
$$

$$
\begin{aligned}
&+\frac{\sigma_0 e^{-2T\kappa}}{24T^3\kappa^3}T\kappa\Big(-e^{2T\kappa}(f_1^2-2f_2-1)T^3\kappa^2\sigma_0^2\Big)\\
&+\frac{\sigma_0 e^{-2T\kappa}}{24T^3\kappa^3}T\kappa\Big(-e^{2T\kappa}(2f_1^2+6f_1-4f_2-8)T^3\kappa^2\sigma_0^2\Big)z^2\\
=\sigma_0\frac{e^{-2T\kappa}}{24T^3\kappa^3}\Bigg[&12\sqrt{2}e^{T\kappa}f_1g_1\alpha\kappa^{3/2}(e^{T\kappa}(T\kappa-1)+1)\rho\sigma_0T^2\\
&-T\kappa\Big[e^{2T\kappa}(f_1^2-2f_2-1)T^3\kappa^2\sigma_0^2\\
&\quad-6g_2\alpha^2(2e^{2T\kappa}T^2\kappa^2-5e^{2T\kappa}T\kappa+T\kappa-8e^{T\kappa}+6e^{2T\kappa})\rho^2\Big]\\
&\quad-6g_1^2\alpha^2\Big[\big(2e^{2T\kappa}T^3\kappa^3(\rho^2-1)+(-9\rho^2e^{2T\kappa}+\rho^2+5e^{2T\kappa}-1)T^2\kappa^2\\
&\qquad-2(e^{T\kappa}-1)(-7\rho^2e^{T\kappa}+\rho^2+3e^{T\kappa}-1)T\kappa-4\rho^2(e^{\kappa T}-1)^2\big)\Big]\\
&+z^2\Big[-12\sqrt{2}e^{T\kappa}g_1\alpha\kappa^{3/2}(e^{T\kappa}(T\kappa-1)+1)\rho\sigma_0T^2\\
&\quad-T\kappa\Big[e^{2T\kappa}(2f_1^2+6f_1-4f_2-8)T^3\kappa^2\sigma_0^2\\
&\qquad-6g_2\alpha^2(4e^{2T\kappa}T\kappa+8e^{T\kappa}-6e^{2T\kappa}-2)\rho^2\Big]\\
&\qquad-6g_1^2\alpha^2\Big[(12\rho^2e^{2T\kappa}-4e^{2T\kappa})T^2\kappa^2+8\rho^2(e^{\kappa T}-1)^2\\
&\qquad\quad-2(e^{T\kappa}-1)(11\rho^2e^{T\kappa}-\rho^2-3e^{T\kappa}+1)T\kappa\Big]\Big]\Bigg],
\end{aligned}
$$

which is the exact approximation used in Jäckel and Kahl (2008).

A.2.3 Local Volatility

As can be seen above, a local and stochastic volatility model contains two $\hat{\sigma}_{i,\mathrm{sl}}$ terms. In Kahl (2007), the derivation of an implied volatility for a purely local volatility model is presented. The expansion is done in terms of an SDE incorporating only local volatility,

$$dx_t = \sigma_0 f(x_t)dW_t,$$

in using the same methodology as before. The first two $\hat{\sigma}_{i,\mathrm{l}}$ terms translate directly to the purely local volatility terms in the expressions (A.17) and (A.20) (that is, the terms which do not contain any form of a function for stochastic volatility, g). The second two terms, $\hat{\sigma}_{3,\mathrm{l}}$ and $\hat{\sigma}_{4,\mathrm{l}}$ are incorporated into the approximation in order to better encapsulate the effect that local volatility has on the implied volatility. These

two terms,

$$\hat{\sigma}_{3,\mathrm{l}} = \frac{T^{3/2} z \sigma_0^4}{48}\Bigg[- f_1^3 + f_1^2 + (2f_2+3)f_1 - 2f_2 + 2f_3 - 3 \\ + 2z^2\Big[f_1^3 + f_1^2 + (4-2f_2)f_1 - 2f_2 + f_3 - 6\Big]\Bigg],$$

$$\hat{\sigma}_{4,\mathrm{l}} = -\frac{T^2\sigma_0^5}{5760}\Bigg[8z^4\Big(19f_1^4 + 15f_1^3 + (20-46f_2)f_1^2 + 6(3f_3 - 5f_2 + 15)f_1 \\ 40f_2 + (16f_2^2 + 15f_3) - 6f_4 - 144\Big) \\ 2z^2\Big(11f_1^4 + 30f_1^3 + (20-44f_2)f_1^2 + 6(12f_3 - 10f_2 - 45)f_1 \\ + 140f_2 + (44f_2^2 - 60f_3) + 36f_4 + 209\Big) \\ - 3\Big(3f_1^4 - 2(6f_2+5)f_1^2 + 16f_3f_1 + 12f_2^2 + 20f_2 + 8f_4 + 7\Big)\Bigg],$$

are presented in Section 4.2.4 of Kahl (2007). For a local stochastic volatility model, the above two terms are denoted as $\hat{\sigma}_{i,\mathrm{l}} = \hat{\sigma}_{i,\mathrm{sl}}$.

The resulting expressions for $\hat{\sigma}_{1,\mathrm{sl}}$, $\hat{\sigma}_{2,\mathrm{sl}}$, $\hat{\sigma}_{3,\mathrm{l}}$ and $\hat{\sigma}_{4,\mathrm{l}}$ are identical to the $\hat{\sigma}_{i,\mathrm{sl}}$ terms (for $i = 1, 2, 3, 4$) given in Jäckel and Kahl (2008).